Materials Science and Engineering R 81 (2014) 1–19

Contents lists available at ScienceDirect

Materials Science and Engineering R

journal homepage: www.elsevier.com/locate/mser

# Nanostructured titanium-based materials for medical implants: Modeling and development

Leon Mishnaevsky Jr.[a,*], Evgeny Levashov[b], Ruslan Z. Valiev[c], Javier Segurado[d], Ilchat Sabirov[d], Nariman Enikeev[c], Sergey Prokoshkin[b], Andrey V. Solov'yov[e], Andrey Korotitskiy[b], Elazar Gutmanas[f], Irene Gotman[f], Eugen Rabkin[f], Sergey Psakh'e[g,h], Luděk Dluhoš[i], Marc Seefeldt[j], Alexey Smolin[g,h]

[a] Technical University of Denmark, Department of Wind Energy, Risø Campus, Frederiksborgvej 399, DK-4000 Roskilde, Denmark
[b] National University of Science and Technology "MISIS", Moscow 119049, Russia
[c] Institute of Physics of Advanced Materials, Ufa State Aviation Technical University (IPAM USATU), Ufa 450000, Russia
[d] IMDEA Materials Institute, Calle Eric Kandel 2, Getafe, 28906 Madrid, Spain
[e] FIAS, Goethe-Universitaet Frankfurt, Ruth-Moufang-Strasse 1, 60438 Frankfurt am Main, Germany
[f] Technion, Department of Materials Engineering, Technion City, Haifa 32000, Israel
[g] Institute of Strength Physics and Materials Science of the Siberian Branch of the Russian Academy of Sciences (ISPMS SB RAS), Tomsk 634050, Russia
[h] Tomsk State University (TSU), Tomsk 634050, Russia
[i] Timplant Ltd., Sjednocení 77/1, CZ72525 Ostrava, Czech Republic
[j] KU Leuven, Departement MTM, Kasteelpark Arenberg 44, B-3001 Heverlee, Leuven, Belgium

ARTICLE INFO

*Article history:*
Available online

*Keywords:*
Ultrafine grained titanium
Medical implants
Computational modeling
Severe plastic deformation
Thermomechanical processing
Nitinol

ABSTRACT

Nanostructuring of titanium-based implantable devices can provide them with superior mechanical properties and enhanced biocompatibity. An overview of advanced fabrication technologies of nanostructured, high strength, biocompatible Ti and shape memory Ni–Ti alloy for medical implants is given. Computational methods of nanostructure properties simulation and various approaches to the computational, "virtual" testing and numerical optimization of these materials are discussed. Applications of atomistic methods, continuum micromechanics and crystal plasticity as well as analytical models to the analysis of the reserves of the improvement of materials for medical implants are demonstrated. Examples of successful development of a nanomaterial-based medical implants are presented.
© 2014 Elsevier B.V. All rights reserved.

**Contents**



*Abbreviations:* ABAQUS, commercial finite element software; ARB, accumulative roll bonding; CP, crystal plasticity; DFT, density functional theory; ECAP, equal channel angular pressing; ECAP-C, equal channel angular pressing – conform; FE, finite elements; GB, grain boundary; HE, hydrostatic extrusion; HPT, high pressure torsion; GGA, generalized gradient approximation; LDA, local density approximation; MCA, movable cellular automata; MD, molecular dynamics; MLPs, martensite lattice parameters; $MTLS_{MAX}$, maximum martensitic transformation; MUBINAF, multicomponent bioactive nanostructured films; NEGB, non-equilibrium grain boundary; PDA, post-deformation annealing; RSEM-RVE, representative volume element (micromechanics of materials); PIRAC, powder immersion reaction assisted coating; $RRS^{PC}$, lattice strain resource recoverable strain; SEM, scanning electron microscopy; SPM, scanning probe microscopy; SPD, severe plastic deformation; TEM, transmission electron microscopy; UFG, ultra fine grained; UMAT,VUMAT, ABAQUS user subroutines; VPSC, visco-plastic self-consistent model; TJR, total joint replacements; XRD, X ray diffraction.

* Corresponding author.
*E-mail address:* lemi@dtu.dk (L. Mishnaevsky Jr.).

http://dx.doi.org/10.1016/j.mser.2014.04.002
0927-796X/© 2014 Elsevier B.V. All rights reserved.

## 1. Introduction

Due to rapid changes in the age structure of the world's population, an increasing number of people need their failed tissues to be replaced by artificial implantable devices. Metallic materials (primarily titanium and cobalt chrome alloys) are widely used for surgical prostheses, such as joint replacements, mechanical heart valves and dental implants. Although conventional materials technology has resulted in clear improvements in implant performance and longevity, rejection or implant failures still happen. The increase in average life expectancy, as well as rapid advances in modern surgery require new generations of clinically relevant biomaterials, with enhanced biological and mechanical performance. Advances in titanium manufacturing technologies are expected to play an important role in the development of the next generation of medical implants.

As forecast by a US Industry Study [1], titanium and titanium alloys will provide the best growth opportunities among biocompatible metals in the years to come and will extend applications in joint replacement systems, dental implants, fusion cages, stents, mechanical heart valves, etc.

Nanostructuring by different processing techniques is one of the promising directions in the development of Ti-based biomaterials with advanced properties. Computational modeling and numerical testing can partially replace the expensive, time- and labor-consuming mechanical and biological experiments and bring nanostructured Ti-based materials closer to clinical realization.

## 2. Titanium as a material of choice for medical implants

For many decades, metallic biomaterials have been used extensively for surgical implants due to the good formability and high strength and resistance to fracture that this class of materials can provide. The important disadvantage of metals, however, is their tendency to corrode in physiological conditions, and a large number of metals and alloys were found unsuitable for implantation as being too reactive in the body. Therefore, the list of metals currently used in implantable devices is limited to three main systems: iron-chromium-nickel alloys (austenitic stainless steels), cobalt-chromium-based alloys, and titanium and its alloys [2,3].

The advantages and drawbacks of metals used for implant fabrication are presented in Table 1. From the point of view of corrosion resistance, Ti is superior to other surgical metals, due to the formation of a very stable passive layer of $TiO_2$ on its surface. Ti is intrinsically biocompatible and often exhibits direct bone apposition. Another favorable property of Ti is the low elastic modulus (twofold lower compared to stainless steel and Co–Cr), which results in less stress shielding and associated bone resorption around Ti orthopedic and dental implants. Furthermore, titanium is more light-weight than other surgical metals and produces fewer artifacts on computer tomography (CT) and magnetic resonance imaging [4–7].

The static and fatigue strengths of titanium, however, are too low for commercially pure titanium (cp-Ti) implants to be used in load-bearing situations. The addition of alloying elements, such as aluminum and vanadium, allows for a significant improvement of the mechanical properties of titanium. Currently, Ti–6Al–4V is the most widely used surgical Ti alloy. Despite the excellent passivity and corrosion resistance of Ti–6Al–4V, elevated concentrations of metal ions were detected in the tissues around the implants, as well as in serum, urine, and remote tissue locations [8]. This slow passive dissolution and accumulation of Al and V ions has long aroused concerns regarding the long-term safety of Ti–6Al–4V alloy implants. Aluminum is an element involved in severe neurological, e.g. Alzheimer's disease, and metabolic bone diseases, e.g. osteomalacia, whereas vanadium ions were shown to be potentially cytotoxic [9,10]. Moreover, accelerated release of Al and V ions is expected to occur in tribocorrosion situations, due to the simultaneous action of corrosion and wear [11]. Given their inadequate wear resistance, Ti alloys are not used in conditions of sliding contact, e.g. in articulating components of total joint replacements. In many clinical situations, however, such as femoral stem/ball contact of modular implants, stem/bone interface of cementless implants or dental implant/bone interface, enhanced release of Al and V ions from Ti–6Al–4V can take place due to fretting (tribocorrosion involving micromotions). Therefore, much effort is being directed toward the development of V- and Al-free Ti alloys. The research on titanium alloys composed solely of non-toxic elements has been under way for several years [12].

**Table 1**
Overview of metals used for implantable medical devices.

| Metal/alloy | Advantages | Drawbacks |
|---|---|---|
| Stainless steel 316 L | High ductility, good machinability, high wear resistance. | Fatigue strength lower than of other implant alloys. High elastic modulus (possibility of stress shielding). Inferior corrosion resistance and biocompatibility compared to other implant alloys. Relatively high metal ion release and adverse host response. |
| Cobalt–chromium (CoCr) based alloys | High static and fatigue strength. High wear resistance. High corrosion resistance and good biocompatibility. | High elastic modulus (possibility of stress shielding). Less corrosion resistant and biocompatible than Ti alloys. Adverse host response to released metal ions (Ni, Cr). |
| Commercially pure (cp) titanium | Excellent corrosion resistance, better than of any other implant metal (due to $TiO_2$ surface oxide). High biocompatibility, direct bone apposition. Relatively low elastic modulus | Static and fatigue strength too low to be used in load-bearing implants. Poor wear resistance. |
| Ti–6Al–4V alloy | Excellent corrosion resistance. High biocompatibility, direct bone apposition. High static and fatigue strength. Relatively low elastic modulus | Poor wear resistance. The release of Al and V ions may cause health problems. |
| NiTi (Nitinol) | Shape memory and superelastic effects. Low stiffness. Good corrosion resistance and biocompatibility. | Adverse host response to released Ni ions. Poor wear resistance. Complex fabrication process. |

An alternative approach to overcome the problem of harmful ion release is to abandon the alloying concept altogether and to enhance the mechanical properties of pure titanium by nanoscale grain refinement. The feasibility of strengthening different metals by nanostructuring has been demonstrated in several studies [13,14]. In addition to improved mechanical properties, a more favorable cell response to nanostructured compared to coarse grained titanium has been reported [15,16].

A special group of Ti alloys that is gaining popularity in many biomedical applications are Ni–Ti alloys (Nitinol) based on the equiatomic intermetallic compound NiTi and containing 54–60 wt.% Ni. Nitinol exhibits the unique properties of shape memory and superelasticity that are utilized in stents, guide-wires, embolic protection filters and other peripheral vascular devices [17–19]. Due to the high titanium content, Nitinol alloys exhibit good biocompatibility and corrosion resistance in vivo. At the same time, the release of Ni ions is a concern as they may cause allergic and carcinogenic effects as well alter cell behavior [20,21].

In addition to shape memory, Nitinol, in its martensitic state, exhibits a very low elastic modulus – less than half that of pure titanium. This makes Nitinol an attractive candidate material for orthopedic, spinal and dental implants since low stiffness minimizes the stress shielding of the peri-implant bone. These new applications will require enhanced mechanical and physical properties (higher strength, tighter transformational hysteresis, etc.). It has been reported in several papers that nanostructuring of Nitinol can lead to a significant improvement in its shape memory and strength characteristics [22–25].

To summarize, the use of titanium-based implantable devices has become an integral part of modern medicine. Nanostructuring is a promising way to further improve the safety, effectiveness and longevity of medical implants made of these materials.

## 3. Nanostructuring of titanium and Ti alloys: concept and technologies

### 3.1. Nanostructuring of titanium and Ti alloys

Nanostructuring of titanium and Ti alloys opens new possibilities for improving the long-term performance of medical implants [26–28].

Still, requirements toward nanostructuring technologies to be used for the production of medical implants are rather high. The technologies should allow the efficient and affordable fabrication of bulk samples with homogeneous microstructures, without any defects. The nanostructured specimens should retain their microstructures even after the samples are coated or installed.

One of the most efficient methods of fabrication of bulk nanocrystalline materials is the metalworking technology called "severe plastic deformation" (SPD) [13]. The SPD concept is based on the fact a metal specimen subjected to high plastic strains with complex stress state, very high hydrostatic pressure and very high strains leading to breaking the coarse grains down into ultra-fine (with a size of 100–1000 nm) or nano-sized (with the size less than 100 nm) grains. Thus, the SPD has been referred to as 'top-down' approach. The main techniques of SPD processing of metals include:

(1) Equal channel angular extrusion (ECAP). The ECAP technique imposes large plastic deformation on a large billet by simple shear [29]. The billet is pressed through a special die which has two channels having the same cross sections and intersecting at an angle in the range of 90–120°. The billet can be subjected to several ECAP passes in order to increase the total strain introduced into the billet. It should be noted that the ECAP-Conform technique was developed in the last decade for producing very long rods [29–31].
(2) High pressure torsion (HPT). In HPT, a small disk is placed between two anvils and one of them is able to rotate under pressure of several GPa, thus, deforming the disk by pure shear [32]. Even hard to deform metallic materials can be subjected to HPT processing due to very high pressures applied. Two shortcomings of this SPD technique include small size of the specimens which can be processed and microstructure inhomogeneity along the disk radius [32].
(3) Accumulative roll bonding (ARB). It is a method of rolling a stack of metal sheets, which is repeatedly rolled to a severe reduction ratio, sectioned into two halves, piled again and rolled [33]. It should be noted that ARB involves not only deformation, but also bonding (roll bonding). Only sheets can be produced via ARB method.
(4) Hydrostatic extrusion (HE) is another technique which has been utilized for grain refinement in metallic materials. In the HE process, the billet is surrounded by a pressurized liquid, except the area of contact with die [34]. This process can be done hot, warm, or cold, however the temperature is limited by the stability of the fluid used. The process must be carried out in a sealed cylinder to contain the hydrostatic medium. The main advantages of the HE processing are absence of any friction between the container and the billet and even flow of material. This allows faster processing speeds, higher reduction ratios, and lower billet temperatures.

**Table 2**
Mechanical properties of nanostructured titanium and Ti-based alloys produced via various SPD techniques compared to cp-Ti and conventional Ti–6Al–4V alloy.

| Material | Processing method | Grain size | $\sigma_{0.2}$ [MPa] | $\sigma_{UTS}$ [MPa] | $\varepsilon_u$ [%] | $\varepsilon_f$ [%] | Reference |
|---|---|---|---|---|---|---|---|
| cp-Ti (grade 2) | Conventional | Several microns | 275 | 345 | | 20 | [49] |
| cp-Ti (grade 4) | Conventional | Several microns | 485 | 550 | | 15 | [49] |
| Ti | ECAP | 280 nm | 640 | 710 | – | 14 | [38] |
| Ti (grade 2) | ECAP + cold rolling | 150–200 nm | 970 | 1080 | 2.4 | 32 | [38] |
| Ti (grade 2) | ECAP + forging + drawing | 50–300 nm | ~1000 | ~1080 | – | – | [41] |
| Ti (Grade 4) | ECAP-C + swaging | 150 nm | 1190 | 1250 | 1.6 | 11 | [42] |
| Ti | HPT | 120 nm | 790 | 950 | | 14 | [43] |
| Ti (Grade 4) | ECAP + swaging + drawing | 200 nm | 1220 | 1280 | 3.7 | 10.1 | [48] |
| Ti–6Al–4V | Mill annealed | Several microns | 795–875 | 860–965 | | 10–15 | [49] |
| Ti–6Al–4V | ECAP + extrusion + annealing | 250 nm | 1310 | 1370 | 4.0 | 12.0 | [44] |
| Ti–6Al–4V | Multiple forging | 200–300 nm | 1180 | 1300 | 0.5 | 7 | [45] |
| $Ti_{74}Nb_{26}$ | ECAP | 200–300 nm | – | 750 | 1–2 | 7–8 | [46] |
| $Ti_{49.4}Ni_{50.6}$ | HPT + annealing | 20–30 nm | 1570 | 2620 | – | 6 | [47] |
| $Ti_{49.8}Ni_{50.2}$ | ECAP | – | 1360 | 1410 | – | 23 | [50] |
| $Ti_{49.8}Ni_{50.2}$ | ECAP + cold rolling | – | 1900 | 2000 | – | 10 | [50] |

Many other SPD processing techniques have been developed [29] and a detailed list of these methods can be found in a recent comprehensive overview [35]. Application of all these technologies lead to the formation of high density of crystal lattice defects in the microstructure, their rearrangement into cells and subgrains, followed by increase of misorientation of low angle grain boundaries into high angle grain boundaries and, thus, formation of ultra-fine- or nano-grained microstructure [13,36,37]. Various SPD methods have been successfully applied for grain refinement in pure Ti and Ti-based alloys [27,37,38–47].

In Table 2, the mechanical properties of bulk nanostructured titanium and several Ti-based alloys produced via various SPD techniques are given. These data clearly demonstrate that the strength characteristics of pure nanostructured titanium are significantly higher than those of cp-Ti of the same grade and are comparable with (and in many cases, higher) those of commercial Ti–6Al–4V alloy. Importantly, the ductility of nanostructured titanium and Ti–6Al–4V is only slightly compromised by the SPD processing.

Severe plastic deformation is also an effective tool for fabricating ultra-fine grained (UFG) and nanostructured Ti–Ni (nitinol) SMAs which exhibit enhanced mechanical properties. In addition, grain refinement down to ultra-fine scale has been shown to affect the phase transformation temperatures of Nitinol [51–54]. NiTi alloys subjected to HPT and ECAP demonstrate high recovery stresses and shape recovery of up to 10% [55], along with higher plateau stress and reduced fracture strain.

Alternatively to SPD processing, bulk nanocrystalline titanium and Ti alloys can be fabricated from nanosize powders, by high pressure consolidation at temperatures close to ambient. In this process, also called Cold Sintering, the high applied pressure results in severe plastic shear deformations of powder particles that are consolidated into a fully dense bulk material [56–58]. The fabrication of dense nanostructured Fe, Ni, Al and Cu metals, as well as Ni–TiC and Cu–TiN nanocomposites by cold sintering of the corresponding nanosize powders was reported [59,60]. In Ref. [61], micron-submicron Ni, Co and Fe intermetallics were fabricated by solid state synthesis of cold sintered elemental nanopowder blends. Full density and high mechanical properties were reported for cold sintered nanostructured rapidly solidified powders of Al alloys and high speed steels [62].

As seen from the above, nanostructuring of Ti-based materials for medical implants can provide them with improved mechanical properties and biocompatibility. SPD-based technologies have proven effective in the processing of nanostructured titanium, nitinol and other Ti-based alloys and already find their way into the dental implant industry [27]. Still, further developments in the current nanostructuring technologies of Ti-based alloys are required to make these materials suitable for other demanding medical applications, such orthopedic, spine and cardiovascular surgeries.

In this and following sections, we describe some works directed toward the optimization of SPD technologies for the fabrication of nanostructured Ti and Ti-based implants. Furthermore, we review methods of computational modeling of nanoscale mechanisms of plastic deformation, strength and biocompatibility of nanostructured Ti and Ti alloys.

### *3.2. Severe plastic deformation: processing routes and microstructure evolution. Multiscale computational modeling*

The formation of nanocrystalline structures in titanium specimens is a result of high hydrostatic pressure and shear stresses of titanium rods under SPD treatment. The quality of the nanostructures, grain size distribution, average grain sizes, grain boundary properties and other microstructural parameters strongly depends on the parameters of thermo-mechanical processing (temperature, strain rate, pressure, etc.).

In order to study the interrelationships between the SPD processing parameters and formed microstructures, multiscale computational models of the SPD process are employed. A number of models considering the engineering aspects of SPD, and, on the other side, the dislocation and nanoscale mechanisms of microstructure evolution under SPD have been developed (see overviews e.g. [63–65]). In order to study the macro-micro-nano and technology-physics interrelations in the SPD process, a multiscale model of SPD process was developed [66]. First, the plastic flow of the material during SPD (ECAP) was modeled using Deform 3D software, with real technological parameters. This allowed one to evaluate the stress and strain fields. It was concluded that the strain intensities in a billet in the longitudinal and cross section was rather uniform at the chosen parameters of ECAP.

Further, a multiscale FE model has been developed, which allowed one to analyze the evolution of microstructure (grain size, dislocation density, vacancy concentration) and texture as well as mechanical properties in pure Ti after ECAP-C processing leading to formation of nanostructure.

On the macro-level, a FEM-model for ECAP-C processing of Ti was developed which takes into account various processing parameters (die-set design, temperature, friction coefficient, processing speed, processing route, etc.). On the meso-level, a CP model (visco-plastic self-consistent model) was used to calculate texture evolution in pure TI during ECAP-C processing as well as to simulate deformation behavior of polycrystalline Ti under given loading condition. This procedure provides informa-

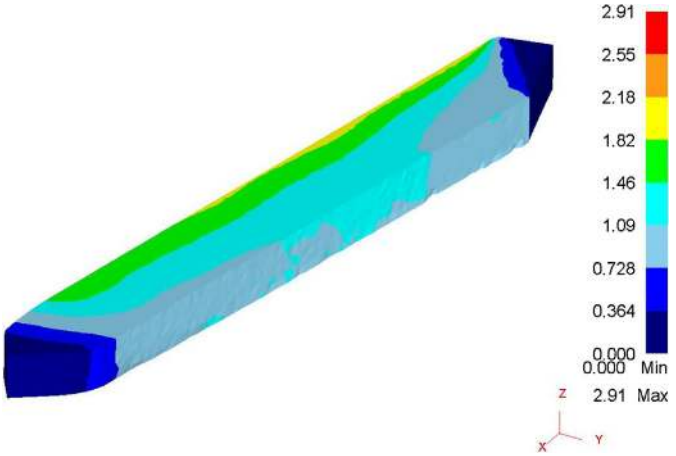


**Fig. 1.** Distribution of shear strain in Ti billet after 4 ECAP-C passes.

tion on slip system activity and output textures affecting mechanical properties of the material.

On the micro-level, a disclination criterion for grain subdivision has been developed taking into consideration the grain refinement process which leads to formation of nanostructure in the processed Ti. These three approaches have been coupled into one unified simulation scheme where deformation history from the macro-level and the data on grain subdivision from the micro-level have been used in VPSC modeling procedure on meso-level. The nanostructured Ti was described using the kinetic dislocation approach, which allowed to obtain information on the microstructure parameters (grain size, dislocation density) and mechanical properties (strength and ductility).

Fig. 1 illustrates distribution of shear strain in a Ti billet after 4 ECAP-C passes obtained from the FEM-model. It is seen that shear deformation is quite homogeneously distributed along the processed billet.

Further, the modeling of deformation behavior and microstructure evolution was performed for nano-Ti produced via ECAP-C for 6 passes with and without extra drawing. It was found that the nano-Ti after ECAP-C processing and drawing shows higher yield strength due to higher total dislocation density. However, this material has a lower ductility due to the lower density of mobile dislocations in the grain interior.

In the nano-Ti obtained via ECAP-C processing and drawing, the increase of vacancy concentration during sample deformation is lower compared to that in the nano-Ti obtained via ECAP-C processing. The vacancies play a more important role in annihilation of dislocations during plastic deformation of the ECAP-C processed and drawn nano-Ti. The non-equilibrium character of grain boundaries increases during plastic deformation due to increasing density of grain boundary dislocations; the density of forest dislocations increases, too.

The main mechanism of the nanoscale structure formation during severe plastic deformation is the grain subdivision. In Ref. [67], a computational model of grain subdivision based on the balance equations for the evolution of dislocation and disclination densities with accumulated plastic strain was developed. These equations include physically based terms for the generation, storage and annihilation rates of the respective lattice defects. It was assumed that orientation fragmentation during the deformation is triggered by intragranular strain localizations. Prismatic, basal and pyramidal slip as well as screw and edge dislocations are treated separately; partial disclination dipoles arise from intersections of slip bands with grain boundaries. Scaling laws are used to calculate cell and fragment sizes from the immobile dislocation and disclination densities. The model allows reproducing substructural parameters in the order of magnitude that is found experimentally after large strains, and predicts the onset of massive orientation fragmentation.

### 3.3. Novel thermomechanical ECAP processing route for fabrication of nano-Ti with very homogeneous structure and superior properties

The analysis of the data presented in Table 2 shows that application of complex SPD processing routes consisting of 2–3 operations (for example, ECAP combined with cold rolling, ECAP combined with swaging and drawing, etc.) leads to smaller grain size and, thus, to higher mechanical strength. In order to improve the technology of nanotitanium rod fabrication to satisfy the requirements for the dental implants, a novel complex SPD processing route for fabrication of high strength nano-Ti was very recently developed on the basis of the computational analysis of the fabrication regimes and structure evolution relationships [42]. The newly developed technology foresees that Ti billets with cross section of 11 mm × 11 mm are subjected to ECAP-C processing at 200 °C for 6 passes followed by drawing at 200 °C into cylindrical rod having a diameter of 6 mm. Thus, obtained rods show the yield strength of 1190 MPa and ultimate tensile strength of 1250 MPa at room temperature and these properties are retained at temperature of human body. Such significant increase of mechanical strength was related to formation of a very homogeneous ultrafine grained microstructure with equiaxed grains having the average grain size of ~150 nm and to development of a crystallographic fiber texture with the c-axis perpendicular to the rod axis and (10–10) direction parallel to the rod axis (Fig. 2). The latter was confirmed via crystal plasticity modeling of drawing process in this processing route [68]. This new processing route for producing nano-Ti was also simulated using the polycrystalline simulation. The model initial conditions were the texture of the billets after 6-ECAP passes assuming a high angle GB misorientation between grains. The drawing process was then simulated and the results showed that the polycrystalline CP models were able to accurately predict the final texture, mechanical anisotropy and grain shape evolutions in rods [68].

From the viewpoint of commercialization, this new SPD processing route is characterized by relatively low cost due to the fact that ECAP-C is a continuous processing technique developed for fabrication of long-length (up to 3 m) rods, so the wastage of material in this processing operation is dramatically reduced [29,30]. It should be also noted that no additional metalforming operations are required for fabrication of dental implants from the processed rods: The near net-shape parts can be readily cut off from the processed rods and machined into dental implants with low wastage of material. So, the newly developed technological route represents a promising approach for the development of stronger Ti-based materials for medical implants.

### 3.4. Thermomechanical treatment of UFG Ti–Ni alloys

As shown in Refs. [23–25,69], the nanosubgrained and nanocrystalline shape-memory alloys (SMA) structures can be efficiently fabricated with the use of the technology called TMT (thermomechanical treatment [70–75]). This technology comprises of cold working (CW) and post-deformation annealing (PDA). The TMT represents in fact a version of ECAP, where the loading conditions are defined by large applied strains at rolling (instead of pressure and numbers on runs, defined in ECAP). To analyze the structure of TMT-processed Ti–Ni SMA, TEM studies of the materials after TMT were carried out. It was observed that a cold rolling (CR) with moderate deformation (true strain $e = 0.3–0.5$) of Ti–Ni SMA creates a well-developed dislocation substruc-

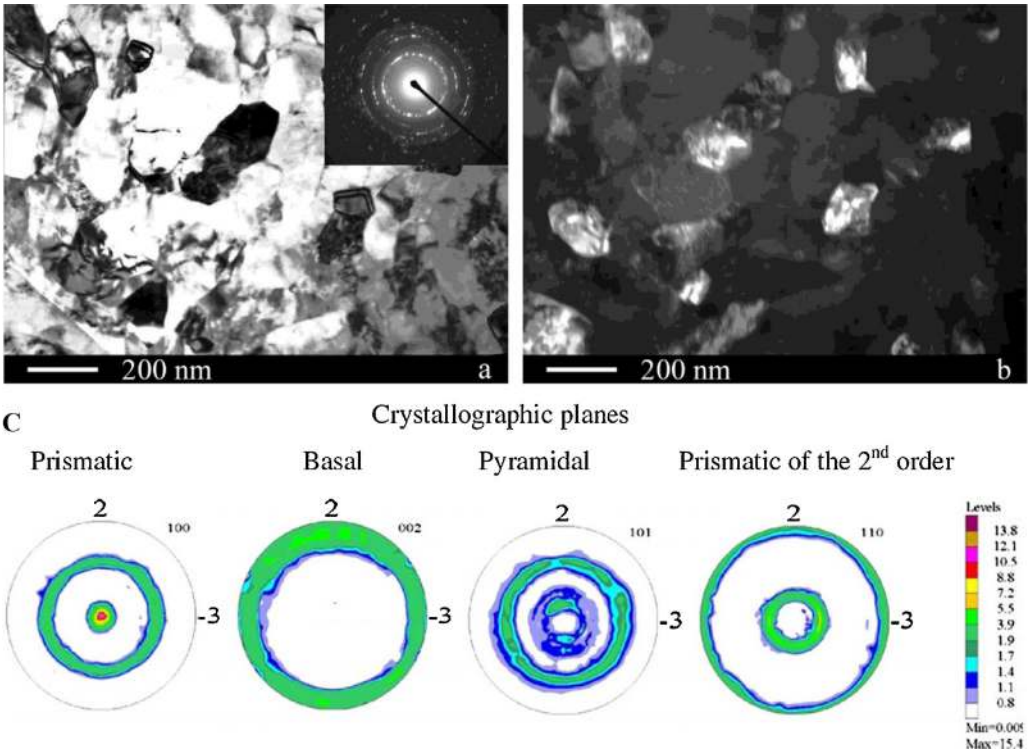


**Fig. 2.** Microstructure and texture of commercially pure Ti after ECAP-C processing in 6 passes and drawing: (a) bright field image; (b) dark field image of the same place; (c) experimental pole figures (10–10), (0 0 0 2), (10–11) and (11–20).

ture of B2-austenite, which is gradually replaced by a mixed nanocrystalline plus amorphous structure during further deformation [72,73]. The PDA in a certain temperature range leads to nanostructures formation (Fig. 3; here is Ti-50.26 at.% Ni SMA annealed at 400 °C for 1 h after CR with various strains in the range from $e = 0.3$ to 1.9). A nanosubgrained polygonized substructure with subgrain size below 100 nm forms as a result of polygonization in the dislocation substructure of moderately deformed alloy, while a nanocrystalline structure with grain size below 100 nm forms as a result of the amorphous phase crystallization and initial nanograin growth in the severely deformed alloy [72]. PDA after CR with intermediate strains creates a mixed nanosubgrained + nanocrystalline structure (fifty-fifty when CR strain is about $e = 0.75$–1.0). Such TMT regimes drastically increase strength parameters and both maximum recovery stress and completely recoverable strain, the latter are the main functional properties of SMA (Fig. 4). Thus, TMT allows to obtain the nanocrystalline Ti-based shape memory allots, with enhanced strength and mechanical properties.

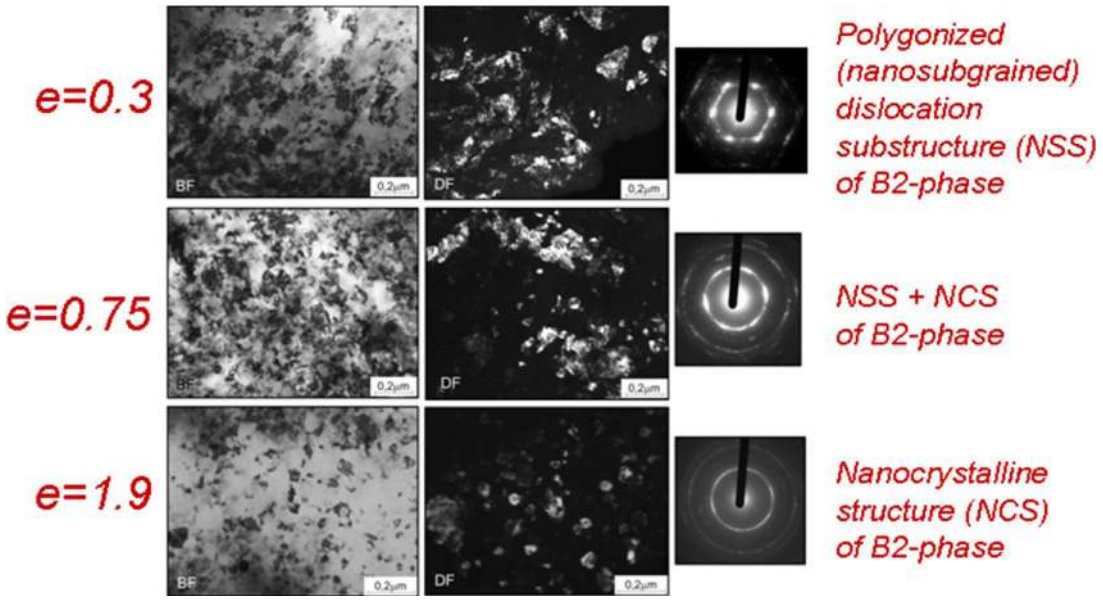


**Fig. 3.** Typical structure for Ti–Ni alloy after cold rolling ($e = 0.3$–1.9) and post-deformation annealing at 400 °C (in Ti–50.26%Ni).

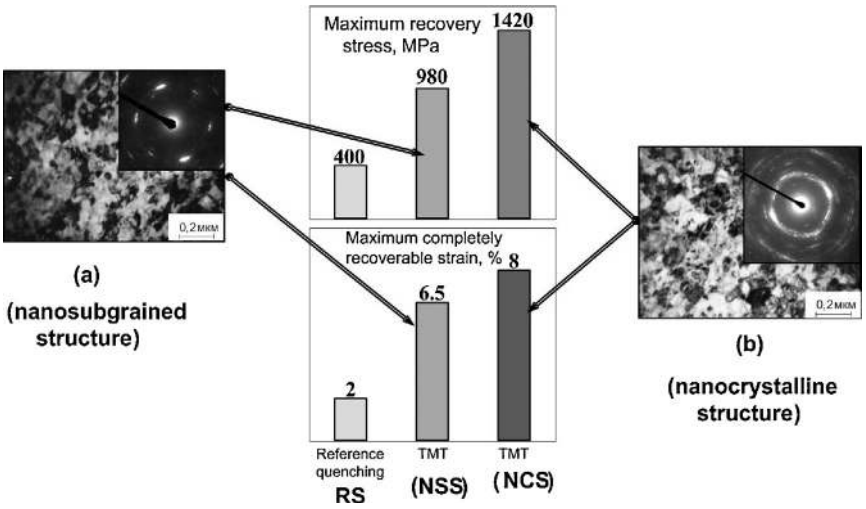


**Fig. 4.** Functional properties of Ti-50.0%Ni alloy with recrystallized (RS), nanosubrained (NSS) and nanocrystalline (NCS) structures.

### *3.5. Comparison of cold sintering and ECAP processing routes of nanostructuring Ti-based materials*

As it was mentioned in Section 3.1, cold sintering or high pressure consolidation of powders at temperatures close to ambient resulting in severe plastic shear deformations and in many cases in full density [56–58] may be an alternative method for processing of nanostructured metals and composites in general and Ti based materials in particular.

In the present research, cold sintering was employed for the processing of submicron-nanoscale pure Ti and NiTi SMA. To produce pure Ti, submicron titanium hydride ($TiH_2$) powder was first compacted to 70% density and dehydrogenated in vacuum at 600 °C for 1 h. Subsequent cold sintering at 300 °C at the pressure of 3 GPa yielded near-fully-dense titanium with grain size in the range 150–250 nm. The microhardness of the obtained specimens was 3600 MPa and their yield strength in compression – 720 MPa. The latter value is close to the yield stress of titanium processed by ECAP [38]. For the processing of NiTi, submicron Ni powder was first treated in hydrogen flow at 300 °C to remove the surface oxide and then blended with submicron $TiH_2$ powder (at 1:1 atomic ratio of Ti and Ni). The blend was then subjected to high energy attrition milling to further refine the submicron $TiH_2$ and Ni particles and to achieve their homogeneous distribution. 70% dense $TiH_2$–Ni compacts were dehydrogenated at 600 °C for 1 h, cold sintered at 3 GPa, 300 °C and vacuum annealed at 700 °C. According to XRD analysis, 4 h at 700 °C were enough to transform the dense blend of Ni and Ti into the NiTi intermetallic (nitinol). The specimens obtained were near fully dense with grain size in the range of 100–150 nm.

The results of our experiments show that cold sintering of ultrafine powders is a feasible route for the fabrication of nanostructured Ti based alloys including nitinol. The potential advantage of cold sintering over ECAP is the possibility of fabricating Ti-based nanocomposites with improved mechanical and biological performance introduction of bioinert and bioactive nanoparticles. The mechanical properties of cold sintered specimens can be further enhanced by subjecting them to severe plastic deformation. More research is needed to optimize the cold sintering processing parameters of nanostructured Ti and Ti based alloys.

## 4. Superior mechanical properties of UFG titanium-based materials: computational modeling

Mechanical and biological properties of nanostructured materials are controlled by a number of physical processes, which act and interact at many scale levels, from atomistic to the macroscopic level, and via various interacting physical mechanisms. The development of new metallic nanomaterials for medical applications and determination of the optimal compositions, fabrication technologies and micro/nanostructures require complex, very expensive and labor consuming experiments along with in vitro (cell culture) and in vivo (animal model) studies.

In order to improve the materials properties, and to determine the optimal microstructures, production regimes and technologies, as well as to reduce animal experimentation, reliable computational models for the virtual, numerical testing of these materials are necessary.

The models, linking the scale levels, physical and mechanical processes with the output service properties of the materials, should provide computational tools for the analysis of the already available and the design of new, improved nanomaterials for medical applications, The models should allow both the predictions of their usability, mechanical properties, biocompatibility, and the optimization, microstructure design and development of new materials on the basis of virtual testing on the materials.

In this section, main approaches and concepts for the computational modeling and virtual testing of nanocrystalline and ultrafine grained materials are considered.

### *4.1. Specific mechanisms of deformation and strength of nanostructured Ti-based materials*

Nanostructured materials are characterized by a number of specific features which distinguish them from regular, coarse grained metals.

Among them, one can mention the following effects: superior yield strength (up to 5–10 times higher than of coarse-grained materials), deviation from Hall–Petch relation at ultrafine and nanoscale grain sizes (below 100 nm), which goes into negative Hall Petch slope at about 10 nm [76,77], high volume of highly disordered grain boundaries, enhanced strain rate sensitivity of mechanical properties, dependent on grain size; asymmetry of tensile and compressive behavior at small grain sizes [78]; superductility at room temperatures, deformation mechanisms different from those the case of coarse grained materials.

Among the observed plastic deformation mechanisms, one can mention, apart from the usual dislocation glide, grain boundary sliding, diffusion controlled creep (Coble model) and Nabarro–Herring creep (through lattice diffusion) [78–81]. These mechanisms

and effect can be observed for different grain sizes and strain rate ranges.

The knowledge of interrelations between nanoscale deformation and strength mechanisms and the service properties of the materials is the way to find the reserves of optimization, improve the fabrication technology or predict the service properties of nanomaterials. When analyzing the mechanical properties of nanostructured metals, one should take into account the peculiar mechanisms of deformation, the role of the grain boundary phase, the mechanisms of grain boundary sliding and diffusional mass transfer.

### 4.2. Atomistic modeling of structure evolution, deformation and properties of ultrafine grained titanium

The straightforward way to simulate the physical and mechanical properties of nanostructured materials is to use atomistic approaches and derive the mechanical and service properties from the atomistic, molecular statics and molecular dynamics simulations.

Most accurate molecular dynamics techniques are based on numerical solution of the Schrödinger equation for the description of interactions within the system (see, e.g., [82,83] and references therein). However, such ab initio approaches are extremely demanding computationally and currently can be performed only for the systems of few hundreds of atoms at the picosecond timescale. An alternative to the ab initio methods are the classical MD simulations which describe the time-evolution of a system by integrating classical equations of motions using the defined interactions between the constituent atoms. Using this technique one can ultimately describe the dynamics of up to $10^7$ atoms at the nano- and microsecond timescales. Within the framework of this scheme the interactions of atoms are parameterized by use of various empirical potentials or the force fields. To a great extent, the success of the MD simulations depends on the availability and reliability of the interatomic potentials. Recently, the MD studies have been carried out to analyze the phase transformations in Ni–Ti alloys [84,85]. In the series of papers [84,86] the structural change in Ni–Ti alloys under martensite and amorphous transformations was analyzed using the interatomic potentials obtained within the frameworks of the embedded atom method (EAM) [87] and of the modified EAM [88]. The EAM potential was built by fitting a number of experimental constants and the values obtained in ab initio calculations [89]. The approach used in Ref. [84] was based on atom-by-atom detection of specific phases by means of common neighbor analysis [90]. In Ref. [97], Yamakov and coworkers carried out the MD simulation of nanocrystalline nickel with the random orientations of the crystals, and the defect-free interiors of the grains. The simulations with $10^5$–$10^6$ atoms were performed. Van Swygenhoven et al. [96] studied the influence of grain boundary structure on plastic deformation of nanostructured Ni and Cu. The MD simulations indicated the presence of a critical grain size below which all plastic deformation was accommodated in the grain boundaries and no intra-grain deformation was observed. Kadau et al. [91] performed a molecular dynamics study of nanocrystalline Al undergoing tensile loading. In Ref. [85,92] (see also [93]) the crystal structure of martensitic NiTi was studied by means of first-principle calculations based several density functional theory (DFT) implementations. The MD was further performed based on the derived interatomic potentials. It was noted that the success of the consequent MD calculations of NiTi alloys strongly depends on the accurate choice of the interatomic Ti–Ti, Ni–Ni, and Ni–Ti potentials. In Ref. [66], a quantum-mechanical evaluation of elastic properties of Ti was carried out on the basis of first principle approach. A set of quantum-mechanical calculations of different crystalline Ti structures were performed using density functional theory (DFT) within a plane-wave pseudopotential approach, implemented in ABINIT package. The exchange and correlations energy functionals were described either within the local density approximation (LDA) or the generalized gradient approximation (GGA). The bulk modulus obtained within GGA + U approach is in agreement with other theoretical calculations and with the experimental data.

In Ref. [94], the deformation mechanisms under tensile loading and indentation, loading rate effect and plasticity initiation were analyzed using the molecular dynamics. In order to include the effect of grain boundaries and interfaces, the authors [94] used a model with a symmetrical tilt grain boundary under tensile loading. The cell size was ~100 Å/40,000 atoms in length. In the simulations it was observed that the potential energy of Ti increases monotonically with deformation up to some threshold strain level. After the initiation and development of plastic deformation, the energy decreases in an avalanche-like manner. With growing loading rate, the rate of potential energy decrease becomes lower, which is attributed to the local structural transformations being incapable of accommodating the growing stress levels in the crystallite. The change in the curve shape observed for the threshold strain level is attributed to the generation of structural defects (dislocations) induced by thermal fluctuations.

Also, the particle method (molecular dynamics approach based on the movable cellular automaton techniques) was applied to study the deformation mechanisms in nanotitanium under nanoindentation [95]. The indentation curve in this case is characterized by a periodic occurrence of kinks, which correlates with the interplanar spacing of the crystallite in the direction of indenter penetration. As soon as the penetration depth of about 4.5 Å is reached, partial dislocations start forming, first under the indenter tip and later on in the glide plane (0 0 0 1) in the direction of crystal side, thereby creating stacking faults and causing steps formation on the free surface.

### 4.3. Micromechanics of ultrafine grained and nanocrystalline titanium and alloys

#### 4.3.1. Composite model of nanocrystalline materials and non-equilibrium grain boundaries

While the atomistic, molecular dynamics methods allow one to analyze the basic, physical properties of the nanomaterials behavior, they can be used still only for modeling relatively small volumes and over small time ranges. That is why there is a necessity to use mechanics methods to simulate the meso- and macroscale nanomaterials behavior and service properties.

In so doing, the main assumption is that the atomistic scale, nanoscale processes can be approximated and modeled by mechanical elements [98,100,101]. This assumption is not apparent, and should be validated by experiments and atomistic simulations.

Quite often, the application of micromechanics in the analysis of nanomaterials is based on the composite model. A material is considered as consisting of two phases: grains with bulk properties and the boundary phase, represented as an amorphous glass material [98,99]. In the series of works based on the composite model, the rule-of-the mixture approach [99], FEM models and unit cells [102,103], other composite models were used. Li et al. [98] developed a phase mixture based finite element model of nanocrystalline nickel, based on the digital topological model of the real microstructure, which followed the experimental observed log-normal distribution and including the rate-dependent amorphous constitutive model for the grain boundary sliding behavior.

An important feature of UFG materials, which has effect on their mechanical and strength properties, is the availability of non-equilibrium grain boundaries. Non-equilibrium grain boundaries (NEGBs) are GBs with higher energies, large area density of GB dislocations, higher diffusion coefficient, larger free volume and

other effects. There are a number of different formulations and explanations of the physics of NEGBs [37,104–107]. Tucker and McDowell [105] characterized the degree of non-equilibrium by excess interfacial free volume (IFV). They demonstrated that the tensile strength is lowered as a function of increasing NE state of GBs. Resistance to GB sliding and migration decreases with increasing IFV, under shear (~30–50% higher peak shear strain for EGB than for NEGB, and 25–30% higher tensile stress). Amouyal and Rabkin determined the relative GB energies in UFG Cu employing the thermal grooving technique and demonstrated that certain degree of non-equilibrium is retained by the GBs even after recrystallization [110].

Part of the NE effect is related to the concentration of alloying elements and formation of precipitates near boundaries, which might increase the critical stresses necessary for nucleation of new dislocations at the boundaries and/or for their motion.

In order to analyze the effect of NEGB on the material deformation, Liu et al. [108,109] studied the influence of changed diffusion coefficient in GBs, high initial dislocation density in GB and the availability of regions of changed properties due to segregation and/or precipitate of alloying elements on the mechanical properties of UFG Ti. The studies were carried out numerically using the composite model of nanomaterials (with grain boundaries as layers of second phase) and the ABAQUS subroutine VUMAT based on the dislocation density evolution model of GB deformation.

The dislocation density based model included the effects of dislocation accumulation and annihilation, local storage (flux of mobile dislocations) and immobilization at stored dislocations, mutual annihilation of dislocations of opposite sign, and, for GBs, a second annihilation mechanism, where two stored dislocations of opposite sign may climb toward each other and annihilate. As a result of the series of numerical simulations, it was demonstrated that the non-equilibrium of GBs leads to the increase in the yield stress. Yield stress increases with decreasing the diffusion coefficient slightly: when the diffusion coefficient increases by factors 100 and 1000 (at the grain size 50 nm), the yield stress increases by 47 and 98%, respectively. An increase in the initial dislocation density (DD) in the GBs by a factor of 1000 (i.e., from $10^{15}$ to $10^{18}$ $m^{-2}$) leads to about 2 times higher yield stress, while the increase by a factor of 100 (i.e., from $10^{15}$ to $10^{17}$ $m^{-2}$) leads to 40% higher yield stress (for *n*Ti with average grain size of 50 nm). The differences are much smaller for the titanium with average grain size of 250 nm: they are roughly 20% and 4%, respectively. Precipitates/foreign atoms (e.g., oxygen and carbon precipitates) in the GB lead to the increased yield stress, by 16% (precipitations randomly arranged in GB) or 28% (precipitations on GB/GI border).

Thus, the micromechanical models of nanomaterials allow to analyze some important effects of the nanomaterials deformation and to explore reserves of the optimization of the materials.

*4.3.2. Crystal plasticity model of UFG Ti*

An important factor influencing the mechanical properties of nanotitanium is the misorientation of grains and the availability of high angle GBs. The modeling of the mechanical behavior of nanomaterials at the level of grains, dislocations and dislocation arrays is carried out with the use of the methods of *crystal plasticity* [111–117]. The introduction of the size effects in the crystal plasticity models has been accomplished through the use of strain gradient single crystal plasticity (SGSCP) models. Nye [118] and Ashby [119] explained the "Smaller is Stronger" phenomenon as the result of the interaction between statistically stored dislocations (SSDs, responsible of plastic strain) and geometrically necessary dislocations (GNDs, responsible of plastic strain gradients). The size effect was simulated with the use of phenomenological strain gradient models that incorporate the influence of a characteristic length of the material in the constitutive equations of isotropic materials [120–123]. This characteristic length was related to some microstructural characteristic as the distance between precipitates, voids, etc. The extension of these phenomenological models to crystal plasticity [124,125] resulted in the so-called "strain gradient crystal plasticity models" that account for both plastic anisotropy and size effects. The size dependency of the plastic flow has a great influence in the mechanical response of polycrystals, and the special characteristics of nano-grained materials cannot be always explained by the dependency of the flow stress with the grain size (Hall–Petch effect).

In Ref. [68], the crystal plasticity approach was used to construct a bottom-up model linking nanoscale to the continuum scale, what will allow taking into account the real microstructures of the material. A crystal plasticity (CP) model of *n*Ti was developed taking into account the grain orientation distribution.

The effective properties of polycrystalline nano-Ti were determined by means of the FE simulation of an Representative Volume Element (RVE) of the microstructure. Two different representation of the microstructure were used: a voxel-based model in which the RVE is made up by a regular mesh of N × N × N cubic finite elements and each of them stands for a Ti grain, and a model where each crystal is represented with many elements (Fig. 5). In either RVE of the polycrystal, the orientation of each grain was determined from the input orientation distribution function (ODF) which describes the initial texture using a Monte Carlo method. The models were validated experimentally.

In order to predict the evolution of texture, the drawing process was simulated. The simulations of nano-Ti billets after 6 ECAP-C passes subject to drawing to produce rods with the longitudinal axis oriented in the billet longitudinal direction were carried out. The analysis showed that the models allow to predict pole figures and microstructure evolution in rods.

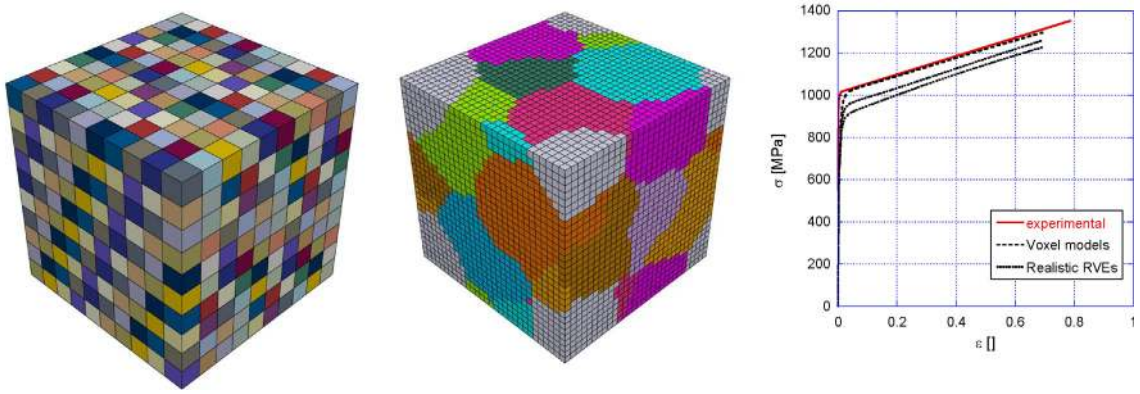


**Fig. 5.** Representative volume elements of polycrystalline Ti. (a) Voxel model with 1000 cubic FE in which each one stands for a single crystal. (b) Realistic RVE containing 100 crystals discretized with 64,000 cubic finite elements. (c) Comparison of curves.

In these investigations, computational models of deformation of UFG titanium at nanoscale were developed, and a number of special effects in plastic deformation in *n*Ti were studied: the effect of orientation distribution, textures, non-equilibrium grain boundaries, diffusion coefficients and precipitates on the deformation behavior, grain subdivision and interaction between grain boundary sliding, diffusion and dislocation nucleation. These models and studies should serve as a basis for further improvement of UFG materials and technologies of their processing.

#### 4.3.3. Grain boundary sliding: analytical modeling

Grain boundary sliding becomes increasingly important in bulk ultrafine grain (grain size in the range 100–1000 nm) and nanocrystalline (grain size below 100 nm) materials, and nanostructured coatings and thin films [126–132]. For example, in the study of Ke et al. [130] relative grain rotations of up to 15° were observed in thin Au films with the average grain size of 10 nm in situ tested in tension in the high resolution transmission electron microscope (TEM) [130]. The absence of any dislocation activity in the film led the authors to the conclusion that GB sliding represents the main room temperature plasticity mechanism in this range of grain sizes. A reversible, non-linear elasticity of thin free-standing Al and Au films was also attributed to grain rotations and GB sliding [131]. These and numerous other observations of GB sliding are backed up by atomistic computer simulations which indicate the increasing role of GB sliding and grain rotations with decreasing grain size in nanocrystalline materials [133–135]. GB sliding, together with Coble creep controlled by GB diffusion are often named as the underlying mechanisms responsible for the inverse Hall– Petch effect (the decrease of hardness and yield stress of nanocrystalline material below a critical grain size [136]). An important aspect of plasticity controlled by GB sliding is a necessity to accommodate changing grain shapes. Moreover, the GBs themselves are rarely planar and exhibit numerous facets and undulations, which also can hinder the sliding process. The GB sliding-related shape accommodation can be diffusional, elastic, or plastic. Diffusional accommodation is controlled by the GB diffusion and is closely related to Coble creep. Raj and Ashby developed a model of GB sliding controlled by diffusion accommodation and obtained a relationship for the sliding rate, $du/dt$ [136], which is often employed in estimates of GB sliding contribution to the plasticity of nanocrystalline materials. While plastic accommodation is dominated by the activity of dislocation sources and conventional dislocation glide in coarse grain materials, nucleation and/or glide of partial dislocations (sometimes accompanied by twinning) is a dominating plasticity mechanism in nanocrystalline materials [133–135]. The partials nucleate at the GB, glide very fast through the small grain, and annihilate at the opposite GB. Finally, the elastic accommodation of GB sliding is very important in nanocrystalline materials because of their high yield stress and high level of internal elastic stresses that can be achieved during deformation.

GB sliding can be phenomenologically described as a viscous Newtonian flow. This process, as well as GB dislocation movement involving climb, are thermally activated; that is why GB sliding in coarse grain polycrystals plays a significant role in deformation only at elevated temperatures above approximately $0.4T_m$, where $T_m$ is the melting point of the material.

Since the diffusion coefficients along the triple junction are much higher than along the GBs [137], the triple junctions can provide an additional diffusion route contributing to the accommodation of GB sliding. In Ref. [66], modified equations for the strain rate of nanocrystalline material due to GB sliding were derived. In the simulations, it was shown that dependence of deformation rate on the grain size is stronger in the case of triple junction diffusion controlled sliding than in the case when GB sliding is controlled by the GB diffusion. For example, decreasing the average grain size by a factor of 2 increases the deformation rate by a factor of 16. Further, the GB dislocation nucleation (e.g., Shockley partial dislocation) accompanied by atomic shuffles and stress-assisted free volume migration at the GB was investigated using the developed "toy model" of the GB sliding. With this model, the typical mechanisms and feature of GB sliding were observed, among others, macroscopic shear bands formation at the advanced stages of deformation and the GBs migration due to violation of the conditions of mechanical equilibrium between the GBs caused by dislocations absorption/emission.

### 4.4. Phase transitions in nanostructured nitinol

With view on the enhancement of nitinol properties and development of nanostructuring technologies for SMAs, the development of methods for the property prediction based on information about SMA microstructure and mechanical behavior is of great importance. The crystallographic resource of the recovery strain is determined by the maximum martensitic transformation lattice strain. Two main methods are used for evaluating the transformation lattice strain: calculations based on the phenomenological theory of martensitic transformation [138–140] and on the deformation theory [141–143]. However, both methods are based on certain assumptions: (1) a single crystal approach is considered and (2) changes of martensite lattice parameters with temperature [144–146], composition [144,146], and lattice distortion in nanostructured material and texture formation are not taken into consideration.

In Ref. [66], methods, algorithms and computer programs for calculating the transformation lattice strain in single-crystal and isotropic as well as textured polycrystalline SMA were developed. The above calculations were applied to Ti–Ni and Ti–Nb–(Zr,Ta) alloys.

Nitinol possesses the highest thermomechanical and superelastic properties as compared to other SMA [147–149]. However, the presence of toxic nickel restricts its medical applications. Therefore, there is a constant search for nickel-free SMA compositions that can be used in the corrosive environment of the human body. In this respect, Ti–Nb–Zr and Ti–Nb–Ta SMA containing only biocompatible components seem to be the most promising SMA [150–152]. These alloys are the objects for the calculations and experimental validation together with Ti–Ni SMA.

#### 4.4.1. Martensite lattice parameters and recovery strain in UFG Ti–Ni and Ti–Nb-based alloys: phase transformation theory analysis

The structure evolution, martensitic transformations and recovery strain of the NITI alloys, including ultrafine grained nitinol, have been studied by using first principle approaches [153,154], finite element models [163,164] (see also the next section), and other methods. The micromechanical models seek to include crystallographic, kinetic and microstructural aspects on the phase transformation in SMA, using the continuum mechanics methods [155–160]. Phenomenological models are based typically on thermodynamics approach with macroscopic variables (see, e.g. [161,162].). Recently, Auricchio et al. [165,166] developed a 3D phenomenological constitutive model for shape memory alloys (SMAs), taking into account martensite reorientation and different kinetics between forward/reverse phase transformations, low-stress phase transformations as well as transformation-dependent elastic properties. In Refs. [66,70–75], a method and a computer program for the precise calculation of martensite and austenite lattice parameters from X-ray diffractograms data were developed on the basis of the phenomenological theory of martensitic transformations. This program can build a complete continuous distribution of the stereographic projection of the transformation

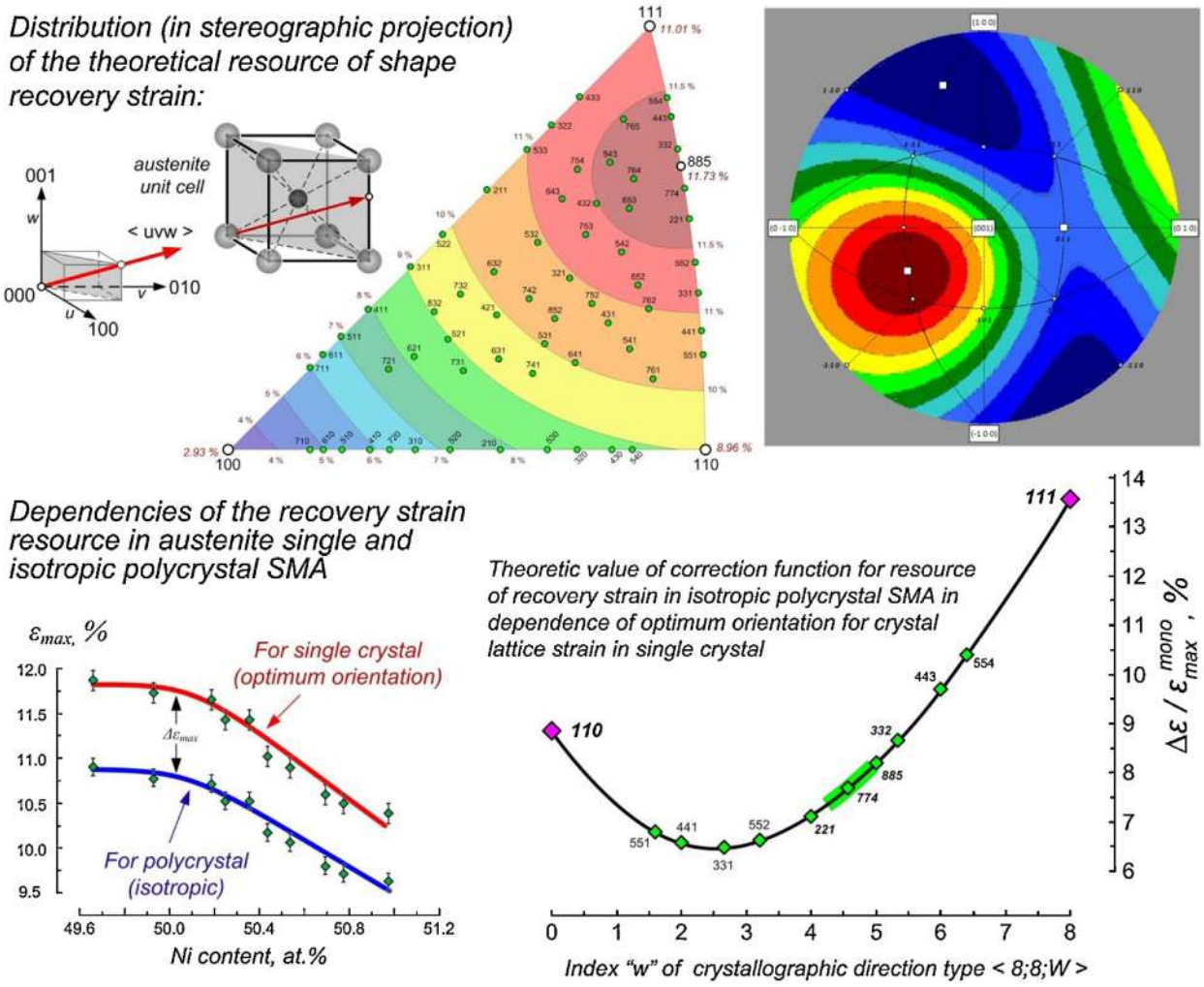


**Fig. 6.** Crystallographic dependence of theoretical resource of shape recovery for Ti-50.0 at.% Ni SMA (in austenite single crystal).

lattice strain which is a theoretical resource of the recovery strain (Fig. 6). The martensite and austenite lattice parameters for Ti–Ni, concentration and temperature dependencies of the maximum transformation lattice strain for all crystallographic directions were determined in an austenite single crystal approach for tension and compression modes. This approach allows to determine the crystallographic resource of the recovery strain, orientation of the maximum recovery strain and maximum transformation lattice strain values for Ti–Ni and Ti–Nb-(Zr,Ta) SMA.

*4.4.2. Thermomechanical modeling of martensitic transformation in nanostructured and UFG nitinol: effect of grain sizes and their distributions*

The nanostructuring represents a promising way to improve the reliability of parts from nitinol. The effect of the grain size on both mechanical properties and martensitic transformations in NiTi alloys has been studied in a number of investigations [167–175]. So, Prokofiev et al. [168] demonstrated that the formation of UFG (ultrafine grained) and NC (nanocrystalline) structures in nitinol leads to the higher strength of the alloy, with narrow hysteresis and low residual strain. Peterlechner et al. [169] observed experimentally that the formation of the martensite is suppressed with decreasing grain size. Burow et al. [170] investigated the effect of various processing routes (ECAP, HPT, wire drawing + annealing) of ultra-fine grained (UFG) microstructures on martensitic transformations using the transmission electron microscopy and differential scanning calorimetry. They observed that all UFG materials show two-step transformations (as different from one-step martensitic transformation on cooling in coarse grained materials). It was also observed that UFG NiTi alloys show strengthening effect and significantly higher functional stability during thermal cycling. Mei et al. [171] studied the nanostructured NiTi with a graded surface nanostructure, and demonstrated that the elastic modulus of nanostructured NiTi increases dramatically with increasing the grain size. They explained it by the suppression of stress-induced martensitic transformation in nanostructured NiTi. In the works by the Austrian group [172–175], mechanisms of deformation of nanocrystalline NiTi were investigated using various experimental (e.g., transmission electron microscopy (TEM) and high resolution transmission electron microscopy (HRTEM)) and theoretical methods. Karnthaler et al. [172] have shown that severe plastic deformation of NiTi leads to amorphization of the material, caused by plastic shear instability initiated at shear bands. In their further investigations, Waitz et al. [173] studied the effect of high pressure torsion (HPT) deformation on the properties of nanocrystalline NiTi, and have shown that with decreasing grain size, the energy barrier" for martensite transformation increases. The martensitic transformation is suppressed in the materials with grains below 60 nm.

In order to determine the conditions and nanostructuring effect on the shape memory effect numerically, the authors of [176]

simulated martensite phase transitions in nanocrystalline NiTi using the finite element method and the thermodynamic theory [177–180]. The finite element model of martensitic phase transitions, based on the approach from [180], includes the strain softening due to martensitic phase transition and scale (grain size) dependent material parameters. In the simulations, it was demonstrated that the energy barrier for martensitic phase transformation in nanocrystalline nitinol increase drastically with decreasing the grain size [179].

Further, it was observed in the FE simulations that the volume content of martensitic phase decreases drastically with reducing the grain size. When the grain size is smaller than some critical value (around 50–80 nm, both in our simulations and in experimental data), the martensitic phase transformations are totally suppressed. On the basis of the comparison of graded and localized distributions of grain sizes of nitinol with homogeneous grain size distribution, it was observed that the martensite rich regions form first on the border between the coarse and fine grained regions, and expand inside the region with small grains along the shear band direction. In the case of gradient microstructures, the effect is controlled not so by the relative gradient of grain sizes, but rather by absolute grain sizes. In this case, the nanostructured grains on the surface will probably prevent the martensite formation (if they are below 50–80 nm), while the large grains inside might undergo phase transitions if the high enough stress is transferred to them.

In this section, the effect of nanostructuring on martensitic phase transformations and mechanical properties of Ti–Ni SMA was studied. It was concluded that the volume fraction of martensitic phase decreases with reducing the grain size. However, grain refinement leads to significant increase of mechanical strength.

## 5. Biocompatibility and coatings for nanometal based implants

### 5.1. Biocompatibility of nanocrystalline Ti-based metals

#### 5.1.1. Biocompatibility and corrosion behavior of Ti-based nanomaterials

Nanocrystalline metals and alloys are characterized by their extremely small grain sizes and correspondingly high volume fraction of grain boundaries, which gives rise to unique physical, chemical and mechanical properties compared with those of the corresponding materials with conventional grain size. However, the effect of nanostructuring on the corrosion behavior has not been adequately studied. For metallic biomaterials, good corrosion resistance is one of the major factors determining their biocompatibility. When metallic implants are placed in the electrolytic environment of the human body, they become the site of electrochemical reactions that lead to the release of metal ions into the surrounding tissues and, in rare cases, to the loss of implant functional ability. Pure Ti and Ti based alloys have inherent corrosion resistance due to the spontaneous formation of a passivating oxide layer. For pure Ti, the layer is a highly protective Ti oxide and the only metal ions that can be released are the ions of Ti. Although generally considered non-toxic, increased concentrations of Ti ions have been shown to decrease the viability of bone and other cells [181,182]. For Nitinol – a near-equiatomic NiTi alloy, the presence of Ni ions in the passive Ti oxide layer results in a less effective corrosion protection and correspondingly lower biocompatibility. Of special concern is the release of Ni ions due to their reported toxic, allergic, and potentially carcinogenic effects [183,184]. Thus, despite a number of successful clinical applications, the biocompatibility of Nitinol still remains controversial [185–187]. The biocompatibility of porous NiTi proposed for use as load bearing scaffolds [188–190] (i.e. the possible effect of NiTi corrosion products on various cells and living tissues) is even more problematic. Given their high surface area and, occasionally, crevice-like pore geometry, NiTi scaffolds can release increased amounts of Ni ions that may cause allergic and carcinogenic effects as well alter cell behavior [149]. Various approaches, such as controlled oxidation [12,191,192] and nitriding [193,194] were proposed to improve the biocompatibility of Nitinol alloys and porous scaffolds.

Grain size decrease down to nanoscale can affect corrosion behavior in several different ways. On the one hand, the high density of intergranular surface defects could lead to a poor corrosion performance since corrosion attack typically initiates at surface heterogeneities. Since grain boundaries typically have a higher energy than the interior of the grain; they will functions as anodic sites. However, for nanocrystalline materials with their extremely high volume fractions of grain boundaries, the atomic compositional difference between the grain interior and the grain boundary caused by atomic segregation can be strongly reduced. This will result in a decrease in the potential difference between the anodic and cathodic sites and lead to a low corrosion rate. For alloys with elements that can form passive films, the atoms of these elements can diffuse easily along grain boundaries to the surface of the alloy to form a protective passive layer. Such preferential diffusion can result in a different (more solute-rich) composition of the passive layer and correspondingly higher corrosion resistance. Slightly lower corrosion rates were reported for nanocrystalline Ti, as well as for electrodeposited nanocrystalline Co coatings compared to their microcrystalline counterparts [150]). The effect of nanocrystallization on the composition of the passive film has been reported for several alloys, including Fe–Cr alloy [195], stainless steel [196] and Ni-based superalloy [197]. For all the nanocrystalline materials, the oxide film was enriched in elements with high affinity for oxygen (Cr and Ti) resulting in enhanced corrosion resistance. Improved corrosion behavior in physiological solution was also reported for nanocrystalline Co–Cr alloy [198]. At the same time, no improvement of corrosion resistance was reported for nanocrystalline titanium [199] and Al–Mg-based alloys [207]. Basing on the limited corrosion data available in the literature for nanocrystalline alloys, it is impossible to conclude how the corrosion behavior of nanocrystalline Ti and TiNi alloys fabricated by severe plastic deformation will compare with the corresponding conventional grain-size materials.

#### 5.1.2. Molecular dynamics modeling of dissolution and ion diffusion from the surface and GBs of Ti–Ni into body fluid

The material dissolution and ion diffusion from the surface of titanium-based materials are important factors of biocompatibility of these materials. They were investigated by many authors [200–206]. While in most investigations the passive behavior of Ni–Ti alloys was observed (see e.g. [205]), it is also important to understand and to know the parameters and mechanisms of ion diffusion of NiTi in general case. In Ref. [206], the diffusion process at the interface of nickel and titanium crystals was investigated by performing molecular dynamics (MD) simulations at different temperatures, namely 500, 600 and 700 K (Fig. 7). The diffusion of nickel atoms on the surface of titanium crystal in the presence of aqueous environment atop the nickel surface was studied as well. MD simulations were carried out using MBN Explorer software package [83]. As a result of simulations, it was found the height of the diffusion energy barrier which is 0.501 eV and 0.544 eV for nickel and titanium atoms, respectively. On the basis of the dependence of the diffusion coefficient on temperature, the diffusion coefficient at the temperatures close to the room temperature was estimated. It is equal to $3.45 \times 10^{-8}$ Å$^2$/ps and $1.44 \times 10^{-8}$ Å$^2$/ps for nickel and titanium, respectively. It was further found that after 300 ps at 800 K the nickel cluster

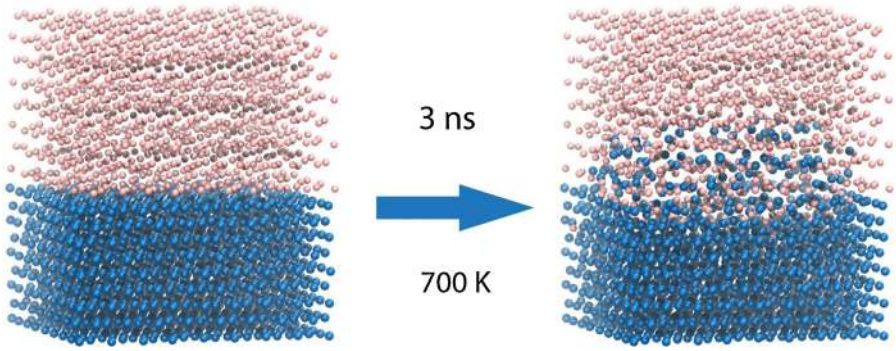


**Fig. 7.** Initial and final structures of the Ni–Ti interface. Titanium and nickel atoms are shown by red and blue colors, respectively. (For interpretation of the references to color in this figure legend, the reader is referred to the web version of the article.)

disintegrates and nickel atoms intercalate under the first layer of titanium crystal. The extrapolation procedure allowed to evaluate the diffusion coefficient of nickel atoms at 310 K as $6.87 \times 10^{-4}$ Å$^2$/ps.

*5.1.3. Experimental study of corrosion and ion release of nanostructured NiTi in physiological solution*

The corrosion and electrochemical behavior of nanocrystalline and micron grain size Nitinol materials was studied in Ringer's solution which simulates physiological (body) fluid. The concentration of Ni and Ti ions in the withdrawn solution was measured by Inductively Coupled Plasma Absorption Emission Spectroscopy (ICP-AES).

For all the Nitinol specimens, the release of Ti ions was always below the detection limit. Practically no Ni release (below or slightly above the detection limit) was measured throughout the experiment for both the coarse- and nanograin $Ti_{49.8}Ni_{50.2}$, as well as for nano-$Ti_{49.4}Ni_{50.6}$ after HPT. All these specimens had a single-phase austenitic (B2) microstructure, and SPD processing had no effect on Ni ion release. In one group of Nitinol specimens, however, relatively high amounts of Ni ions were released both before and after SPD processing. Measurable Ni concentrations were detected as early as 48 h immersion. According to X-ray diffraction analysis, this material had a multi-phase composition, the major phase being austenitic NiTi (B2), and the rest – martensitic NiTi (B19′) and $Ti_2Ni$. In SEM, it was observed that the material was highly non-homogeneous, with numerous inclusions of $Ti_2Ni$ in the NiTi matrix, which must have led to the low corrosion characteristics and high ion release. Again, no effect of SPD processing on Ni ion release was observed. In each Nitinol group (single- and multi-phase), the electrochemical characteristics (corrosion, pitting and repassivation potentials) of nanocrystalline alloys fabricated by ECAP and/or high pressure torsion (HPT) were comparable to those of the corresponding conventional grain size Nitinol.

Fig. 8 shows the cumulative Ni release from nano-Nitinol produced by different SPD processes as compared to coarse-grained Nitinol.

The results obtained show that the corrosion resistance and metal ion release of nanocrystalline Nitinol materials is at least as good as that of their conventional grain size counterparts. This is in agreement with the results reported in Ref. [208] where ultrafine-grained (200–300 nm) $Ni_{50.8}Ti_{49.2}$ prepared by ECAP technique exhibited a corrosion behavior similar to that of the commercial coarse-grained material. This means that nanocrystalline alloys are biocompatible and can be used for human body implantation. At the same time, to maintain adequate corrosion behavior of NiTi, it is highly important that the microstructure is homogeneous, with no second phase inclusions. Basing on the presented results, as well as

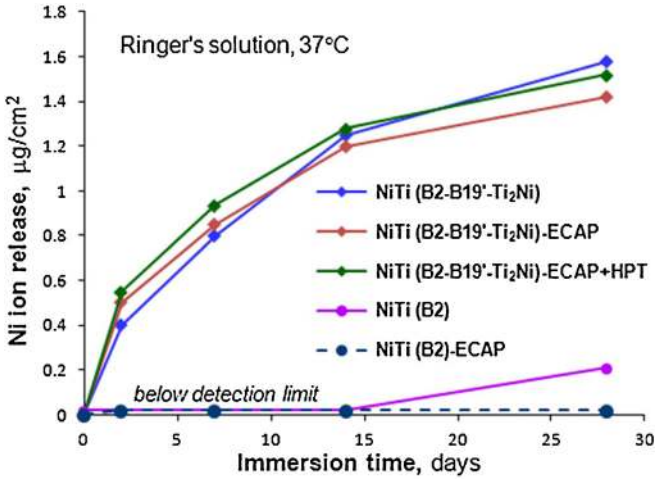


**Fig. 8.** Cumulative Ni release from nano-Nitinol produced by different SPD processes as compared to coarse-grained Nitinol.

on the limited literature data available, it was assumed that the high volume fraction of grain boundaries in nanocrystalline Ti-based alloys doesn't lead to enhanced corrosion and dissolution, presumably due to the highly passive nature of the titanium oxide surface layer. Moreover, it is plausible that nanostructuring promotes the formation of the Ti oxide film, due to the high density and hence availability of short-circuit diffusion paths. The structure and chemical composition of the surface oxide (albeit only several to tens of nanometers thick) are among the main factors determining the corrosion behavior of biomedical Ti-based alloys. The effect of enhanced transport along titanium nanograin boundaries on the oxide characteristics requires further investigation.

*5.2. Bioactive coatings and their effect on the mechanism of deformation*

*5.2.1. Role of bioactive coatings in Ti-based implants*

While the most important requirements to the permanent hard tissue replacements are long term performance and stability, Ti has poor tribological properties and tends to undergo severe wear, making it unsuitable for articulating implant components. Host response to wear debris has been implicated as the main cause of aseptic loosening and premature failure of total joint replacements.

Titanium is not bioactive and does not bond directly to the bone, what can lead to small shifting and loosening of the implant. Further, toxic and carcinogenic ions (like Ni from Ti–Ni and Al and V from Ti–6Al-4V) can be in some cases released into the body

environment and may initiate long-term health problems, such as Alzheimer disease, neuropathy and osteomalacia.

An effective way to promote the formation of a bone-like layer on the implant surface, prevent toxic ion release, and improve mechanical and tribological characteristics is the deposition of multifunctional bioactive film. Recently, a new approach to the design of thin-film biomaterials for medical applications has been developed [210,211]. Multifunctional bioactive nanostructured films (MuBiNaFs) were deposited by magnetron sputtering of composite targets based on nonstoichiometric titanium carbide $TiC_{0.5}$ with various inorganic additives (CaO, $TiO_2$, $ZrO_2$, $Si_3N_4$, $Ca_3(PO_4)_2$, and $Ca_{10}(PO_4)_6(OH)_2$) [212,213]. Also microarc method of applying coatings on the surface of metal implants is quite technological and allows the formation of thick porous coating, which promotes intensive ingrowth of bone tissue into the surface of the implant [214,215].

Multifunctional bioactive coatings accelerate the adaptation of implants in human bodies and improve their performances. Multifunctional bioactive nanostructured films (MuBiNaFs) which are deposited using magnetron sputtering of composite targets, demonstrate high hardness, fatigue and adhesion strength, reduced Young's modulus, low wear and friction, high corrosion resistance with high level of biocompatibility, bioactivity, and biostability, and, thus, are promising candidates as protective films on the surface of metallic implants such as orthopedic prostheses, materials for connective surgery and dental implants.

*5.2.2. Deformation and strength of bioactive coatings*

In Ref. [209], mechanisms of deformation of multicomponent bioactive nanostructured films (MUBINAF) and protective wear resistant TiN coatings on the substrate of various biocompatible Ti-based nanomaterials (Ti, Ti-alloy with shape memory effect, and Ti-alloy with superelasticity effect) were investigated under mechanical loading expected in implants.

Analyzing the indents in uncoated samples using Scanning Electron (SEM) and Scanning Probe (SPM) microscopy, one observed only homogeneous deformation at indentation. In contrast, the MUBINAF TiCaPCON/substrate system shows a very specific mechanical behavior. The parameter $H^3/E^2$ (hardness/Young modulus ratio, which defines the mechanism of plastic deformation in materials), determined for the TiCaPCON/substrate systems, was varied from 0.32 (TiNi) to 0.4 (Ti) and to 0.55 (TiNbZr). Practically, it means the non-monotonic deformation mechanisms and the formation of inhomogeneous mechanism involving the formation of shear bands under indentation. Indeed, a system of steps parallel to indent faces as well as cracks was observed in the indents. In case of the coatings deposited on SMA substrates (TiNi and TiNb-based), the appearance of shear bands is less pronounced. It may be connected with pseudo elastic recovery of the SMA substrates compared to that made of micro and nanostructured pure titanium. In fact the depth of imprint is about twice less for MUBINAF onto shape memory substrates (MDTNT2) than for MUBINAF onto ns-Ti (MDT3). It should be noted also that steps on the profile are larger at MDT3 system and more fine for MDTNT2 one.

It can be concluded that deposition of TiCaPCON coating not only improves the mechanical properties (hardness, Young modulus, elastic recovery) but also changes a mechanism of localized deformation in the near-surface layers. Deformation was found to proceed inhomogeneously, through formation of shear bands during penetration of a Vickers diamond indenter. Formation of shear bands is most pronounced in case of substrates with higher $E$ and lower elastic recovery ($R$), such as ms-Ti ($E$ = 125–130 GPa, $R$ = 10–12%). In the dynamic impact testing experiments, the relationships between generally critical loads (loads, at which a coating starts to fracture) and number of cycles were studied. During these experiments all the samples (MUBINAF, deposited onto micro- and nanostructured Ti-based substrates, namely Ti, shape memory alloy Ti–Ni, Ti–Nb–Ta and Ti–Nb–Zr) were tested for three different durations: $10^4$, $5 \times 10^4$ and $10^5$ cycles, to plot the fatigue curves. It can be clearly seen that in case of Ti–Nb–Ta and Ti–Nb–Zr substrates behavior and values of the MUBINAF critical loads do not considerably depend on the substrate structure and material. In contrast, MUBINAF, deposited onto Ti and Ti–Ni substrates, exhibited an evident dependency on the substrate structure. For example, MUBINAF critical loads for nanostructured Ti–Ni substrates were 2.5 times higher than those of microstructured ones for all numbers of impacts. The MUBINAF on Ti showed different behaviors depend upon substrate material structure, but overall the coating, deposited onto microstructured substrate, performed better in the tests

*5.2.3. Multilevel modeling of strength and failure of nanostructured bioactive coatings on Ti-based biomaterials*

The strength and failure of coatings on the Ti-based implants are controlled by the mechanics of thin film/ductile substrate systems, as reviewed in Ref. [216]. The main mechanisms of coating failure in this case (cracking, decohesion and delamination) are often modeled with the use of analytical fracture mechanics based models, lattice network models, probabilistic models of flaw/crack distribution, stress distribution analysis, which yields periodic stress distributions [216–222]. In Ref. [95], a multilevel model based on the MCA (movable cellular automata [223]) is developed and applied for the computational analysis of mechanical behavior of protective coatings (TiCaPCON) on nanocrystalline Ti-based materials. The simulated cellular automaton model is presented in Fig. 9 as fcc packing of automata. Displacement, automata velocities, stress fields as well as the force-indentation depth curves were obtained for different coating thicknesses and substrate structures, and compared with experiments. It was concluded that deposition of TiCaPCON coating not only improves the mechanical properties (hardness, Young modulus, elastic recovery) but also changes a mechanism of localized deformation in the near-surface layers.

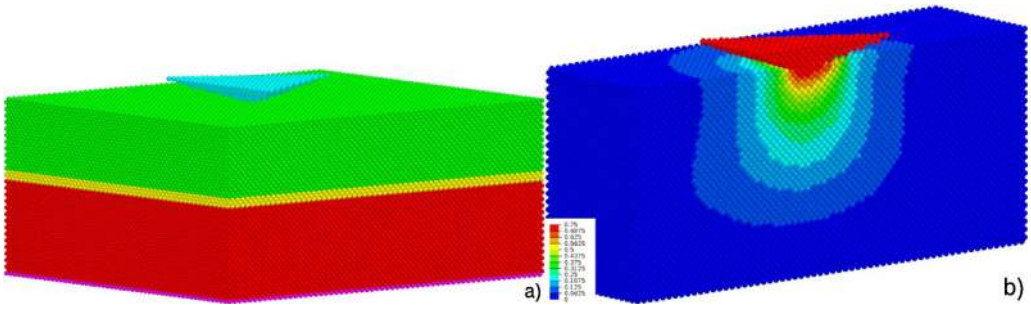


**Fig. 9.** Model for indentation represented by automata packing (a) and field of automata velocities (b, m/s) as a section along the symmetry plane.

Further, the coatings on nanostructured substrates were more resistant to adhesive failures, than the ones on the substrates with coarse-grained microstructure. The coating deposited onto nanostructured Ti–Ni alloy substrate were found to possess the highest adhesive/cohesive strength (27 N and 50 N, respectively), while the lowest ones were for the coating deposited onto coarse-grained titanium and Ti–Nb–Ta substrates.

Summarizing the studies, one can state that the coatings have a great potential to improve strength, reliability and lifetime of implants from nanostructured materials. Still, detailed studies are necessary for each coating/substrate combinations to ensure the optimal use of the potential.

### *5.3. Wear resistant TiN based PIRAC coatings on nanostructured Ti-based alloys*

Despite excellent biocompatibility and biomechanical properties, the use of Ti alloys in implantable devices is limited by their strong susceptibility to abrasive and adhesive wear. Generation and accumulation of wear debris between the sliding implant surfaces or at implant/bone or implant/bone cement interfaces may cause bone resorption jeopardizing the long-term stability of the prosthesis. As a result of their inadequate wear behavior, titanium alloys are not used, for example, as articulating components in total joint replacements, but only as femoral stems, acetabular shells and tibial trays [62,224,225]. The more widespread use of Ti and its alloys in orthopedics, especially as articulating TJR (total joint replacement) components, depends on our ability to improve their wear resistance. Coating Ti alloy implant components with a thin TiN layer is expected to provide them with the required high wear resistance [226,227]. TiN-coated Ti alloy parts are offered as substitutes to the traditional CoCr alloy components in both knee and hip systems for nickel-sensitive patients or where large-diameter femoral heads are indicated (heavy, active patients). A number of techniques can be used for the fabrication of hard TiN coatings, the most commonly used being physical vapor deposition – PVD [226–229]. As the low-temperature PVD process does not generally involve diffusion phenomena and chemical reactions, the adhesion between the substrate and the hard layer is weak. The adhesion is further compromised by high residual stresses associated with ceramic PVD coatings on metal substrates [230]. As a result, delamination and spallation of TiN-PVD coatings from the articulating surfaces of orthopedic implants was observed in in vitro wear simulations, in animal tests and in clinical trials [228,231]. To prevent the failure of TiN coating adhesion, surface modification methods capable of producing a strong TiN coating-substrate interface should be looked for. A new reactive diffusion process called PIRAC (Powder Immersion Reaction Assisted Coating) nitriding has been proposed as an attractive alternative to conventional PVD-based nitriding techniques. In PIRAC, a several micron thick TiN coating is formed by interaction of Ti-based substrate with highly reactive monatomic nitrogen supplied by decomposition of an unstable nitride and/or by selective diffusion of the atmospheric nitrogen. Reactive diffusion of nitrogen atoms into titanium alloy results in the formation of a Ti–N coating. PIRAC nitrided Ti surface consists of a several micrometers thick outer compound layer (TiN–$Ti_2N$) and a several tens of microns thick inner solid solution layer. Beneath the ceramic, a nitrogen-enriched Ti gradually transforms into the metal alloy, preventing an abrupt mismatch in properties. This hardened N-rich titanium layer provides an optimal support for the ceramic coating and prevents its collapse and delamination. The low level of residual stresses in PIRAC coatings on Ti-6Al-4V substrate compared to the PVD TiN layers is an additional factor in the excellent adhesion of PIRAC coatings. In contrast to PVD, PIRAC coatings are not externally applied layers but are grown from the substrate itself and are characterized by an excellent conformity and strong adhesion [232,233]. As PIRAC is not a line-of-sight process, it allows uniform coating of complex shape implant components. TiN PIRAC coated Ti–6Al–4V and NiTi exhibited excellent corrosion resistance reduced metal ion release [193,234]. Moreover, good biocompatibility of TiN PIRAC coated Ti–6Al–4V alloy with both soft and bone tissues was reported in Ref. [235]. However, TiN-PIRAC coatings are typically produced at relatively high temperatures that can cause the coarsening of nanocrystalline structure. Indeed, some coarsening of micron-scale Ti alloy grains was observed after long (192 h) PIRAC nitriding treatments at 700 °C [236]. So, the question arises whether such TiN based PIRAC coatings can be used for protection of nanocrystalline Ti-based implants.

In order to explore the possibility of nanostructure retention in pure Ti and NiTi (nitinol) alloy, relatively short (up to 2 h) PIRAC nitriding treatments of ECAP-processes materials were performed at 600 and 650 °C. As demonstrated by X-ray diffraction analysis (see Fig. 10), titanium nitride (TiN–$T_2N$) based hard coatings were formed on both nanostructured Ti and nitinol. The coatings obtained were approximately 0.3 μm thick, which could be enough to provide good wear resistance. High resolution SEM examination revealed that practically no growth of 100–150 nm nanograins occurred after 100 h exposure of pure Ti at 600 °C and of Nitinol at 650 °C (see Fig. 11). Thus, TiN based reactive diffusion coatings can be grown on nano-Ti and nano-NiTi by PIRAC nitriding at low temperatures while retaining their initial ultrafine nanostructure.

## 6. Potential for application: nanotitanium based implants with small radius

The development of the technology of ECAP producing of UFG titanium with enhanced mechanical properties made it possible to produce dental implants with lower radii. According to the results of the computational analysis, these low radius implants with a diameter of 2.4 mm (Fig. 12) can withstand loads similar to those carried by the implants of conventional design with a diameter of 3.5 mm made from coarse-grained Ti.

Rods of high strength nanostructured Ti (Grade-4) produced by ECAP-C processed followed by drawing were subjected to grinding, in order to produce the required surface quality and tolerance. Cylindrical screw implants with the thread Timplant Nanoimplant and a diameter of 2.4 mm and a length of the intraosseal part 10, 12 and 14 mm were manufactured from UFG Ti. The implant has a polished gingival part with a cone top above it. The developed implant is made from pure Ti and, therefore, it does not contain any

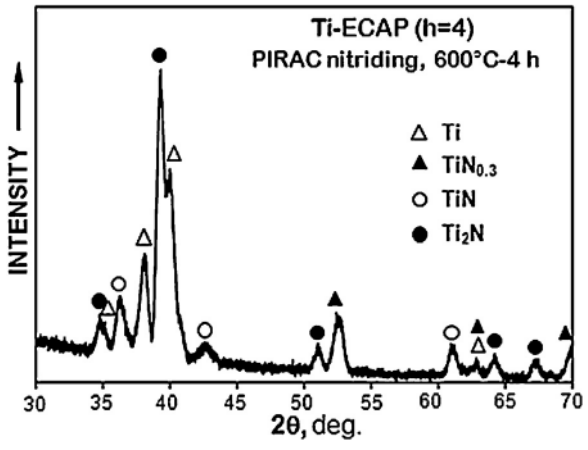


**Fig. 10.** XRD pattern of nano-Ti after PIRAC nitriding at 600 °C, 24 h.

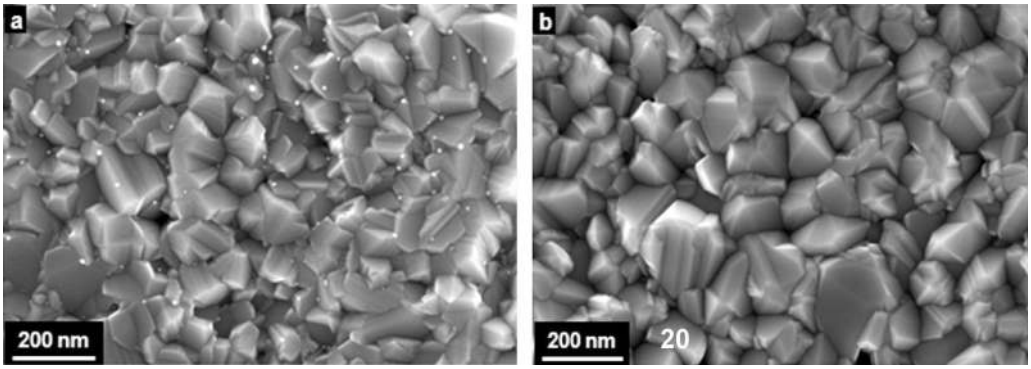


**Fig. 11.** Representative microstructures of nano-Ti: (a) as-produced by ECAP; (b) after PIRAC nitriding at 600 °C for 100 h. High-resolution SEM.

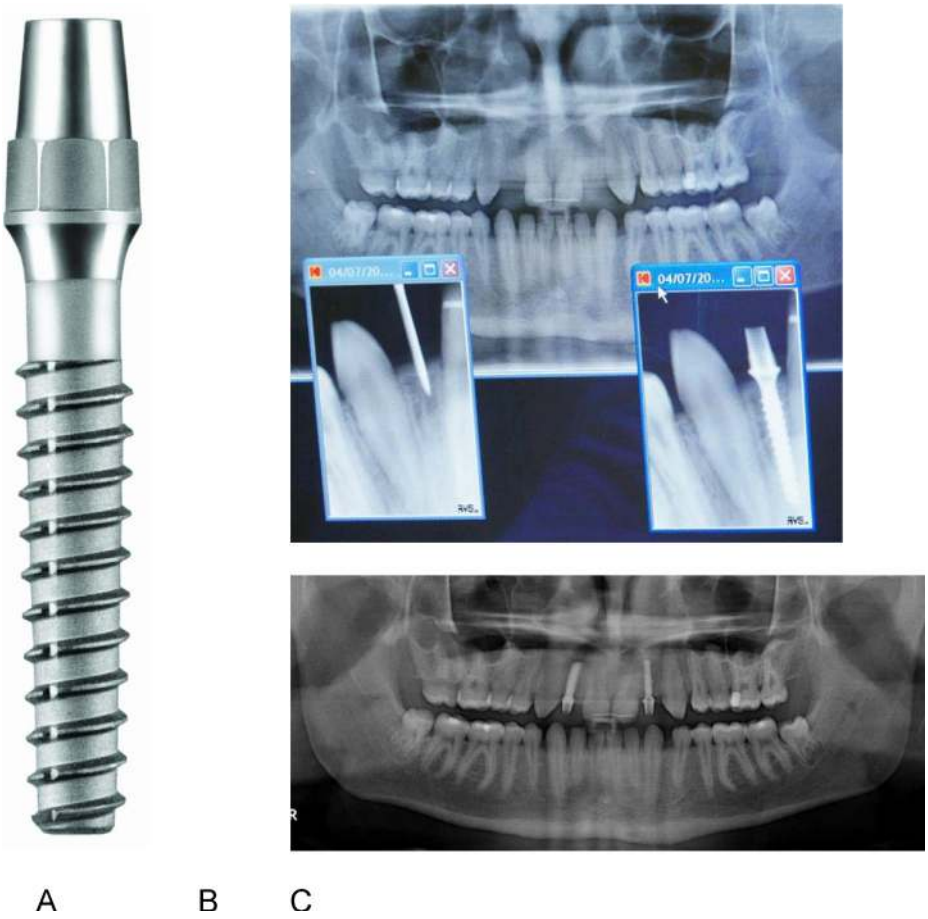


**Fig. 12.** Implant from nanostructured Ti (a) and (b) and (c) X-ray photos after surgery and control photo after incorporation of implants.

toxic alloying elements (like V) and elements classified as allergens (like Ni, Co, or Cr). Another positive side of the low radius implant is that it allows one to minimize medical intrusion, thus, making the implants better bearable. These implants from *n*Ti showed also better biological properties than coarse grained Ti. The healing process is faster and about 70% of nanoimplants could be loaded immediate after inserting.

Further, another implant prototype with diameter of 2.0 mm was developed in the framework of VINAT project. The implant was manufactured from new UFG Ti with increased strength (U.T.S. 1330 MPa). The implant prototype was installed into body of a patient. In the specific situation, the patient (18 years old, with no space for bigger implant) in his mouth, was offered to install the low radius implant (2.0 mm) (between teeth 11 and 13). Another implant with the diameter of 2.4 mm was inserted to the right side position 12. The man left the dental office with two nanoimplants and with two provisional crowns made in the same day as implants were inserted (Fig. 12b and c). After 6 weeks, final metalceramic crowns were fixed on the implants.

Other medical devices developed on the basis of the above studies are a removable clip for clipping blood vessels based on One-Way and Two-Way Shape Memory Effects, while another one is an extractor "Trawl" for concernment removal based on Superelasticity Effect. Their Ti–Ni working elements are made from the thermomechanically treated Ti-50.7 at.% Ni SMA with nanosubgrained structure. The devices had been created and patented in a collaboration between MISIS and "Globetek 2000 Pty Ltd." (Australia). The clinical experiments are currently underway.

## 7. Summary and conclusions

In this review, the application, fabrication, modeling and development of ultrafine grained titanium based materials for implantable devices and other medical applications are discussed. The usability of different materials for surgical implants, nanostructuring technologies for Ti-based materials, methods of computational modeling and virtual testing of these materials and reserves of their optimization are reviewed. Some recently developed technologies of fabrication of nanostructured, high strength, biocompatible materials for medical implants are outlined, among them, a novel thermomechanical processing route for fabrication of nano-Ti with very homogeneous structure and superior properties and thermomechanical treatment of nitinol.

Computational models and tools, developed for the simulation and analysis of ultrafine grained Ti-based materials at different scale levels, are reviewed. These models and tools can be applied to the analysis of peculiarities of the structures of ultrafine grained and nanocrystalline materials and special reserves of their improvement. Among these effects, the effects of orientation distribution, textures, non-equilibrium grain boundaries, diffusion coefficients and precipitates on the deformation behavior, grain subdivision and interaction between grain boundary sliding, diffusion and dislocation nucleation can be mentioned. These models and studies should serve as a basis for further improvement of UFG materials and technologies.

Bioactive coatings on nanocrystalline Ti-based implants are the effective way to promote the formation of a bone-like layer on the implant surface, prevent toxic ion release.

An example of successful development and installation of a prototype, nanomaterial-based dental implant with lower radius which can withstand loads similar to those carried by the implants of conventional design, is presented.

## Acknowledgement

The authors gratefully acknowledge the financial support of the Commission of the European Communities through the 7th Framework Programme Grant "Virtual Nanotitanium" (VINAT, Contract No. 295322) and financial support of the Ministry of Education and Science of the Russian Federation. L.M. and E.L. acknowledge also the financial support of the Ministry of Education and Science of the Russian Federation in the framework of Increase Competitiveness Program of NSTU MISIS,. I.S. acknowledges Spanish Ministry of Economy and Competitiveness for funding through the Ramon y Cajal Fellowship.

## References

[1] Biocompatible Materials, US Industry Study with Forecasts to 2010 & 2015, Study #2111, The Freedonia Group, September 2006, p. 264.
[2] D.H. Kohn, Curr. Opin. Solid State Mater. Sci. 3 (1998) 309–316.
[3] I. Gotman, J. Endourol. 11 (1997) 383–389.
[4] N. Soumya, R. Banerjee, in: R. Narayan (Ed.), ASM Handbook, vol. 23 "Materials for Medical Devices", ASM International, Materials Park, OH, USA, 2012, pp. 6–17.
[5] M. Niinomi, Mater. Trans. 49 (2008) 2170–2178.
[6] M. Geetha, A.K. Singh, R. Asokamani, A.K. Gogia, Prog. Mater. Sci. 54 (2009) 397–425.
[7] M. Long, H.J. Rack, Biomaterials 19 (1998) 1621–1639.
[8] M. Browne, P.J. Gregson, Biomaterials 21 (2000) 385–392.
[9] D. Zaffe, C. Bertoldi, U. Consolo, Biomaterials 25 (2004) 3837–3844.
[10] N.J. Hallab, S. Anderson, M. Caicedo, A. Brasher, K. Mikecz, J.J. Jacobs, J. Biomed. Mater. Res. A 74 (2005) 124–140.
[11] N. Diomidis, S. Mischler, N.S. More, M. Roy, Acta Biomater. 8 (2012) 852–859.
[12] M. Niinomi, Metal. Mater. Trans. A 33 (2002) 477–486.
[13] R.Z. Valiev, Nat. Mater. 3 (2004) 511–516.
[14] I.A. Ovid'ko, T.G. Langdon, Rev. Adv. Mater. Sci. 30 (2012) 103–111.
[15] Y. Estrin, E.P. Ivanova, A. Michalska, V.K. Truong, R. Lapovok, R. Boyd, Acta Biomater. 7 (2011) 900–906.
[16] T.N. Kim, A. Balakrishnan, B.C. Lee, W.S. Kim, B. Dvorankova, K. Smetana, et al. J. Mater. Sci.: Mater. Med. 19 (2008) 553.
[17] T. Duerig, A. Pelton, D. Stöckel, Mater. Sci. Eng. A 273–275 (1999) 149–160.
[18] S.A. Shabalovskaya, Int. Mater. Rev. 46 (2001) 1–18.
[19] C.D.J. Barras, K.A. Myers, Eur. J. Vasc. Endovasc. Surg. 19 (2000) 564–569.
[20] S. Shabalovskaya, J. Anderegg, J. Van Humbeeck, Acta Biomater. 4 (2008) 447–467.
[21] A. Michiardi, C. Aparicio, J.A. Planell, J.F. Gil, J. Biomed. Mater. Res. B 77 (2006) 249–256.
[22] R.Z. Valiev, D. Gunderov, E. Prokofiev, V. Pushin, Y.T. Zhu, Mater. Trans. 49 (2008) 97–101.
[23] V. Brailovski, S. Prokoshkin, I. Khmelevskaya, K. Inaekyan, V. Demers, S. Dobatkin, E. Tatyanin, Mater. Trans. 47 (2006) 795–904.
[24] S. Prokoshkin, V. Brailovski, K. Inaekyan, V. Demers, I. Khmelevskaya, S. Dobatkin, E. Tatyanin, Mater. Sci. Eng. A 481482 (2008) 114–118.
[25] I.Y. Khmelevskaya, S.D. Prokoshkin, V. Dobatkin, E.V. Tatyanin, I.B. Trubitsyna, Mater. Sci. Eng. A 438–440 (2006) 472–475.
[26] R.Z. Valiev, I. Sabirov, A.P. Zhilyaev, T.G. Langdon, JOM 64 (2012) 1134–1142.
[27] R.Z. Valiev, I.P. Semenova, V.V. Latysh, H. Rack, T.C. Lowe, J. Petruzelka, L. Dluhos, D. Hrusak, J. Sochova, Adv. Eng. Mater. 10 (2008) B15–B17.
[28] L. Mishnaevsky, Jr., E. Levashov (Eds.), Selected Publications of the EU FP7 project Virtual Nanotitanium (VINAT) "Theoretical analysis and virtual testing of titanium-based nanomaterials", Comp. Mater. Sci., vol. 76, 2013, pp. 1–2.
[29] R.Z. Valiev, T.G. Langdon, Prog. Mater. Sci. 51 (2006) 881–981.
[30] G.J. Raab, R.Z. Valiev, T.C. Lowe, Y.T. Zhu, Mater. Sci. Eng. A 382 (2004) 30–34.
[31] A. Rosochowski, L. Olejnik, J. Mater. Process. Technol. 125–126 (2002) 309–316.
[32] A.P. Zhilyaev, T.G. Langdon, Prog. Mater. Sci. 53 (2008) 893–979.
[33] Y. Saito, H. Utsunomiya, T. Sakai, R.G. Hong, Scr. Mater. 39 (1998) 1221–1227.
[34] M. Lewandowska, K.J. Kurzydlowski, J. Mater. Sci. 43 (2008) 7299–7306.
[35] Y. Estrin, A. Vinogradov, Acta Mater. 61 (2013) 782–817.
[36] B. Verlinden, Metalurgija 11 (3) (2005) 165–182.
[37] R.Z. Valiev, R.K. Islamgaliev, I.V. Alexandrov, Prog. Mater. Sci. 45 (2000) 103–189.
[38] V.V. Stolyarov, Y.T. Zhu, I.V. Alexandrov, T.C. Lowe, R.Z. Valiev, Influence of ECAP routes on the microstructure and properties of pure Ti, Mater. Sci. Eng. A 299 (2001) 59–67.
[39] I. Sabirov, R.Z. Valiev, I.P. Semenova, R. Pippan, Metall. Mater. Trans. A 41 (2010) 727–733.
[40] V.L. Sordi, M. Ferrante, M. Kawasaki, T.G. Langdon, J. Mater. Sci. 47 (2012) 7870–7876.
[41] J. Gubicza, Zs. Fogarassy, Gy. Krállics, J. Lábár, T. Törköly, Mater. Sci. Forum 589 (2008) 99–104.
[42] D.V. Gunderov, A.V. Polyakov, I.P. Semenova, G.I. Raab, A.A. Churakova, E.I. Gimaltdinova, I. Sabirov, J. Segurado, V.D. Sitdikov, I.V. Alexandrov, N.A. Enikeev, R.Z. Valiev, Mater. Sci. Eng. A 562 (2013) 128–136.
[43] A.V. Sergueeva, V.V. Stolyarov, R.Z. Valiev, A.K. Mukherjee, Scr. Mater. 45 (2001) 747–752.
[44] I.P. Semenova, E.B. Yakushina, V.N. Nurgaleeva, R.Z. Valiev, J. Mater. Sci. 100 (2009) 1691–1696.
[45] S. Zherebtsov, G. Salishchev, R. Galeyev, K. Maekawa, Mater. Trans. 46 (2005) 2020–2025.
[46] J. Ma, I. Karaman, B. Kockar, H.J. Maier, Y.I. Chumlyakov, Mater. Sci. Eng. A 528 (2011) 7628–7635.
[47] R.Z. Valiev, D.V. Gunderov, V.G. Pushin, J. Metastable Nanocryst. Mater. 24–25 (2005) 7–12.
[48] I. Sabirov, M.T. Perez-Prado, J.M. Molina-Aldareguia, I.P. Semenova, G.Kh. Salimgareeva, R.Z. Valiev, Scr. Mater. 64 (2011) 69–72.
[49] M. Niinomi, Mater. Sci. Eng. A 243 (1998) 231–236.
[50] V.G. Pushin, R.Z. Valiev, Y.T. Zhu, S.D. Prokoshkin, D.V. Gunderov, L.I. Yurchenko, Mater. Sci. Forum 503–504 (2006) 539–544.
[51] V.V. Stolyarov, E.A. Prokofiev, S.D. Prokoshkin, S.V. Dobatkin, I.B. Trubitsyna, I.Yu. Khmelevskaya, V.G. Pushin, R.Z. Valiev, Phys. Met. Metall. 100 (2005) 608–618.
[52] S.D. Prokoshkin, I.Y. Khmelevskaya, S.V. Dobatkin, I.B. Trubitsyna, E.V. Tatyanin, V.V. Stolyarov, E.A. Prokofiev, Acta Mater. 53 (2005) 2703–2714.
[53] V.G. Pushin, V.V. Stolyarov, R.Z. Valiev, T.C. Lowe, Y.T. Zhu, Mater. Sci. Eng. A 410–411 (2005) 386–389.
[54] A.V. Sergueeva, C. Song, R.Z. Valiev, A.K. Mukherjee, Mater. Sci. Eng. A 339 (2003) 159–165.
[55] Th. Waitz, C. Tecn. Mat. 20 (2008) 25–29.
[56] E.Y. Gutmanas, A. Rabinkin, M. Roitberg, Scr. Metall. 13 (1979) 11–15.
[57] E.Y. Gutmanas, Powder Metall. Int. 15 (1983) 129–132.
[58] E.Y. Gutmanas, ASM Handbook, vol. 7, "Powder Metal Technologies and Applications", ASM International, Materials Park, OH, 1998, pp. 574–582.
[59] E.Y. Gutmanas, L.K. Trusov, I. Gotman, Nanostruct. Mater. 4 (1994) 893–901.
[60] E.Y. Gutmanas, A. Trudler, I. Gotman, J. Metastable Nanocryst. Mater. 386–388 (2002) 329–334.
[61] E.Y. Gutmanas, I. Gotman, L. Farber, E. Paransky, Proc. Powder Metallurgy World Congress, Kyoto, Japan, (1993), pp. 1148–1151.
[62] E.Y. Gutmanas, Prog. Mater. Sci. 34 (1990) 261–366.
[63] I.V. Alexandrov, R.G. Chembarisova, Rev. Adv. Mater. Sci. 16 (2007) 51–72.
[64] H.S. Kim, Yu. Estrin, Mater. Sci. Eng. A 410–411 (2005) 285–289.
[65] H. Petryk, S. Stupkiewicz, Int. J. Mater. Res. 103 (2012) 3.
[66] L. Mishnaevsky Jr., et al., Theoretical analysis, design and virtual testing of biocompatibility and mechanical properties of titanium-based nanomaterials, EP FP7 VINAT Project Periodic Report, DTU, Roskilde, 2012p. 128.
[67] M.G.C. Seefeldt, Comp. Mater. Sci. 76 (2013) 12–19.
[68] J. Segurado, J. Llorca, Comp. Mater. Sci. 76 (2013) 3–11.
[69] V. Brailovski, S. Prokoshkin, K. Inaekyan, V. Demers, Proc. 8th European Symposium on Martensitic Transformations ESOMAT 2009, 07–11 Septermber 2009,,

EDP Sciences, Prague, 2009, pp. 1–10. , http://dx.doi.org/10.1051/esomat/200901001.
[70] S.D. Prokoshkin, Y. Khmelevskaya, S.V. Dobatkin, I.B. Trubitsyna, E.V. Tatyanin, V.V. Stolyarov, E.A. Prokofiev, Acta Mater. 53 (2005) 2703–2714.
[71] V. Brailovski, S. Prokoshkin, P. Terriault, F. Trochu (Eds.), Shape Memory Alloys: Fundamentals, Modeling and Applications, ETS Publ., Montreal, 2003, , 851 p..
[72] V. Brailovski, S. Prokoshkin, I. Khmelevskaya, K. Inaekyan, V. Demers, S. Dobatkin, E. Tatyanin, Mater. Trans. 47 (2006) 795–804.
[73] S. Prokoshkin, V. Brailovski, K. Inaekyan, V. Demers, I. Khmelevskaya, S. Dobatkin, E. Tatyanin, Mater. Sci. Eng. A 481–482 (2008) 114–118.
[74] V. Brailovski, S. Prokoshkin, K. Inaekyan, V. Demers, J. Alloys Compd. 509 (2011) 2066–2075.
[75] S.D. Prokoshkin, V. Brailovski, A.V. Korotitskiy, K.E. Inaekyan, A.M. Glezer, Phys. Metal. Metall. 110 (2010) 289–303.
[76] J. Li, G.J. Weng, Int. J. Plast. 23 (2007) 2115–2133.
[77] P. Barai, G.J. Weng, Acta Mech. 195 (2008) 327–348.
[78] E. Gürses, T. El Sayed, Mater. Lett. 65 (2011) 3391–3395.
[79] W. Yang, H. Wang, J. Mech. Phys. Solids 52 (2004) 875–879.
[80] B. Zhu, R.J. Asaro, P. Krysl, R. Bailey, Acta Mater. 53 (2005) 4825–4838.
[81] R.J. Asaro, P. Krysl, B. Kad, Phil. Mag. Lett. 83 (2003) 733–743.
[82] S. Hao, B. Moran, W.K. Liu, G.B. Olson, J. Comput. Aided Mater. 10 (2003) 99–142.
[83] I.A. Solov'yov, P.V. Nikolaev, A.V. Yakubovich, V.V. Dick, A.V. Solov'yov, MBN Explorer Users's Guide, Version 1.0.0, FIAS Preprint, 2010 244 pp..
[84] K. Saitoh, K. Kubota, T. Sato, Technische Mechanik 30 (2010) 269–279.
[85] G.J. Ackland, A.P. Jones, R. Noble-Eddy, Mater. Sci. Eng. A 481–482 (2008) 11.
[86] T. Sato, K. Saitoh, N. Shinke, Model. Simulat. Mater. Sci. 14 (2006) S39–S46; T. Sato, K. Saitoh, N. Shinke, Mater. Sci. Eng. A 481–482 (2008) 250–253.
[87] D. Farkas, D. Roqueta, A. Viette, K. Ternes, Model. Simulat. Mater. Sci. Eng. 4 (1996) 359–369.
[88] M.I. Baskes, Phys. Rev. B. 46 (1992) 2727–2742; Y.-M. Kim, B.-J. Lee, M.I. Baskes, M.I. Baskes, Phys. Rev. B 74 (2006) 014101:1–014101:12.
[89] W.S. Lai, B.X. Liu, J. Phys.: Condens. Mater. 12 (2000) L53.
[90] H. Tsuzuki, P.S. Branicio, J.P. Rino, Comput. Phys. Commun. 177 (2007) 518.
[91] K. Kadau, T.C. Germann, P.S. Lomdahl, B.L. Holian, D. Kadau, P. Entel, M. Kreth, F. Westerhoff, D.E. Wolf, Metall. Mater. Trans. A 35 (2004) 2719–2722.
[92] X. Huang, K.M. Rabe, G.J. Ackland, Nat. Mater. 2 (2003) 307–311.
[93] X. Huang, K.M. Rabe, G.J. Ackland, Phys. Rev. B 67 (2003) 024101.
[94] G.B. Sushko, A.V. Verkhovtsev, A.V. Yakubovich, A.V. Solov'yov, J. Phys.: Conf. Ser. 438 (2013) 012021-1–012021-11.
[95] S.G. Psakhie, A.Yu. Smolin, E.V. Shilko, G.M. Anikeeva, Yu.S. Pogozhev, M.I. Petrzhik, E.A. Levashov, Comp. Mater. Sci. 76 (2013) 89–98.
[96] H. Van Swygenhoven, A. Caro, D. Farkas, Mater. Sci. Eng. A 309–310 (2001) 440–444; P.M. Derlet, H. Van Swygenhoven, Scripta Mater. 47 (2002) 719–724.
[97] V. Yamakov, S.R. Phillpot, D. Wolf, H. Gleiter, Acta Mater. 50 (2002) 5005–5020.
[98] S. Li, et al. Comp. Mater. Sci. 45 (2009) 390–397.
[99] J.E. Carsley, J. Ning, W.W. Milligan, S.A. Hackney, E.C. Aifantis, Nanostruct. Mater. 5 (1995) 441–448.
[100] L. Mishnaevsky Jr., Computational Mesomechanics of Composites, John Wiley, London, 2007p. 280.
[101] L. Mishnaevsky Jr., Rev. Adv. Mater. Sci. 30 (2012) 60–72.
[102] H.S. Kim, Scr. Mater. 39 (1998) 1057–1061.
[103] H.S. Kim, C. Suryanarayana, S.J. Kim, B.S. Chun, Powder Metall. 41 (1998) 217–220.
[104] A. Hasnaoui, H.V. Swygenhoven, P.M. Derlet, Acta Mater. 50 (2002) 3927–3939.
[105] G.J. Tucker, D.L. McDowell, Int. J. Plast. 27 (2011) 841–857.
[106] V.N. Chuvil'deev, Non-equilibrium grain boundary in metals, Theory and applications, Fizmatlit, Moscow, 2004.
[107] V.N. Chuvil'deev, V.I. Kopylov, W. Zeiger, Ann. Chim. Sci. Mat. 27 (2002) 55–64.
[108] H.S. Liu, W. Pantleon, L. Mishnaevsky Jr., Comp. Mater. Sci. 83 (2014) 318–330.
[109] H.S. Liu, L. Mishnaevsky Jr., Acta Mater. (2014), http://dx.doi.org/10.1016/j.actamat.2014.03.017.
[110] Y. Amouyal, E. Rabkin, Acta Mater. 55 (2007) 6681–6689.
[111] G.I. Taylor, J. Inst. Met. 62 (1938) 307–324.
[112] R. Hill, J. Mech. Phys. Solids 14 (1966) 95–102.
[113] R. Hill, J. Rice, J. Mech. Phys. Solids 20 (1972) 401–413.
[114] R. Asaro, Advances in Applied Mechanics, vol. 23, Academic Press, New York, 1983.
[115] D. Pierce, R. Asaro, A. Needleman, Acta Metall. 30 (1982) 1087–1119.
[116] J.L. Bassani, T.Y. Wu, Proc. R. Soc. Lond. A 435 (1989) 21–41.
[117] F. Roters, P. Eisenlohr, L. Hantcherli, D.D. Tjahjanto, T.R. Bieler, D. Raabe, Acta Mater. 58 (2010) 1152–1211.
[118] J.F. Nye, Acta Metall. 1 (1953) 153–162.
[119] M.F. Ashby, Phil. Mag. 21 (1970) 399–424.
[120] E.C. Aifantis, J. Eng. Mater. Technol. 106 (1984) 326–330.
[121] N.A. Fleck, J.W. Hutchinson, Adv. Appl. Mech. 33 (1997) 295–361.
[122] N.A. Fleck, J.W. Hutchinson, J. Mech. Phys. Solids 49 (2001) 2245–2271.
[123] W.D. Nix, H. Gao, J. Mech. Phys. Solids 46 (1998) 411–425.
[124] M.E. Gurtin, Int. J. Plast. 26 (2010) 1073–1096.
[125] L. Bardella, J. Mech. Phys. Solids 54 (2006) 128–160.
[126] A.A. Fedorov, M.Yu. Gutkin, I.A. Ovid'ko, Scr. Mater. 47 (2002) 51–55.
[127] S.V. Bobylev, N.F. Morozov, I.A. Ovid'ko, Phys. Rev. Lett. 105 (2010) 055504.
[128] H. Van Swygenhoven, P.M. Derlet, Phys. Rev. B 64 (2001) 224105.
[129] H. Van Swygenhoven, P.M. Derlet, A. Hasnaoui, Phys. Rev. B 66 (2002) 024101.
[130] M. Ke, S.A. Hackney, W.W. Milliga, E.C. Aifantis, Nanostruct. Mater. 5 (1995) 689–697.
[131] A. Haque, M.T.A. Saif, Deformation mechanisms in free-standing nanoscale thin films: a quantitative in situ transmission electron microscope study, Proc. Natl. Acad. Sci. U.S.A. 101 (2004) 6335–6340.
[132] N.Q. Chinh, G. Vörös, P. Szommer, Z. Horita, T.G. Langdon, Adv. Mater. 18 (2006) 34–39.
[133] H. Van Swygenhoven, M. Spaczer, A. Caro, D. Farkas, Phys. Rev. B 60 (1999) 22–25.
[134] V. Yamakov, D. Wolf, S.R. Phillpot, A.K. Mukherjee, H. Gleiter, Nat. Mater. 3 (2004) 43–47.
[135] M.A. Meyers, A. Mishra, D.J. Benson, Prog. Mater. Sci. 51 (2006) 427–556.
[136] R. Raj, M.F. Ashby, Metall. Trans. A 2 (1971) 1113–1127.
[137] M.R. Chellali, Z. Balogh, L. Zheng, G. Schmitz, Scr. Mater. 65 (2011) 343–346.
[138] S. Miyazaki, S. Kimura, K. Otsuka, Y. Suzuki, Scr. Metall. 18 (1984) 883–888.
[139] T. Saburi, M. Yoshida, S. Nenno, Scr. Metall. 18 (1984) 363–368.
[140] T. Saburi, in: K. Otsuka, C.M. Wayman (Eds.), Shape Memory Materials, Cambridge Univ. Press, Cambridge, 1998, p. 57.
[141] L.A. Monasevich (Ed.), Shape Memory Alloys and Their Applications in Medicine, Nauka, Novosibirsk, 1992, , 741 p..
[142] S.D. Prokoshkin, A.V. Korotitskiy, V. Brailovski, S. Turenne, I.Y. Khmelevskaya, I.V. Trubitsyna, Acta Mater. 52 (2004) 4479–4492.
[143] S. Prokoshkin, A. Korotitskiy, A. Tamonov, I. Khmelevskaya, V. Brailovski, S. Turenne, Mater. Sci. Eng. A 438–440 (2006) 549–552.
[144] S.D. Prokoshkin, V. Brailovski, S. Turenne, I.Y. Khmelevskaya, A.V. Korotitskiy, I.B. Trubitsyna, J. Phys. IV 112 (2003) 651–654.
[145] Yu.P. Mironov, S.N. Kulkov, Izvestiya VUZov. Fizika 37 (1994) 49–54.
[146] S.D. Prokoshkin, V. Brailovski, K. Inaekyan, V. Demers, I. Khmelevskaya, S. Dobatkin, E. Tatyanin, Mater. Sci. Eng. A 481–482 (2008) 114–118.
[147] H. Funakubo (Ed.), Shape Memory Alloys, Gordon and Breach Sci. Publ., N.Y., 1975, , 275 p..
[148] K. Otsuka, C.M. Wayman (Eds.), Shape Memory Materials, Cambridge Univ. Press, Cambrigde, 1998, , 284 p..
[149] V. Brailovski, S. Prokoshkin, P. Terriault, F. Trochu (Eds.), Shape Memory Alloys: Fundamentals, Modeling and Applications, ETS Publ., Montreal, 2003, , 851 p; J. Ryhanen, et al. J. Biomed. Mater. Res. 35 (1997) 451–457.
[150] S. Miyazaki, H.Y. Kim, H. Hosoda, Mater. Sci. Eng. A 438–440 (2006) 18–24.
[151] J.I. Kim, H.Y. Kim, T. Inamura, H. Hosoda, S. Miyazaki, Mater. Sci. Eng. A 403 (2005) 334–339.
[152] V. Brailovski, S. Prokoshkin, M. Gauthier, K. Inaekyan, S. Dubinskiy, M. Petrzhik, M. Filonov, Mater. Sci. Eng. C 31 (2011) 643–657.
[153] M.F.-X. Wagner, W. Windl, Acta Mater. 56 (2008) 6232–6245.
[154] Z.-Y. Zeng, C.-E. Hu, L.-C. Cai, X.-R. Chen, F.-Q. Jing, Phys. B: Condens. Matter 405 (2010) 3665–3672.
[155] Q.P. Sun, K.C. Hwang, J. Mech. Phys. Solids 41 (1993) 1–17.
[156] B.C. Goo, C. Lexcellent, Acta Mater. 45 (1997) 727–737.
[157] X. Gao, M. Huang, L.C. Brinson, Int. J. Plast. 16 (2000) 1345–1369.
[158] X. Peng, W. Pi, J. Fan, Int. J. Plast. 24 (2008) 966–990.
[159] V.I. Levitas, I.B. Ozsoy, Int. J. Plast. 25 (2009) 239–280.
[160] X.M. Wang, B.X. Xu, Z.F. Yue, Int. J. Plast. 24 (2008) 1307–1332.
[161] L.C. Brinson, J. Intel. Mater. Syst. Struct. 4 (1993) 229–242.
[162] J.G. Boyd, D.C. Lagoudas, Int. J. Plast. 12 (1996) 805–842.
[163] J. Gemperlova, V. Paidar, F. Kroupa, Czech. J. Phys. 39 (1989) 427–446.
[164] C. Grossmann, A. Schaefer, M.F.-X. Wagner, Mater. Sci. Eng. A (2009) 1172–1178.
[165] F. Auricchio, R.L. Taylor, J. Lubliner, Comput. Methods Appl. Mech. Eng. 146 (3–4) (1997) 281–312.
[166] F. Auricchio, E. Bonetti, G. Scalet, F. Ubertinic, Int. J. Plast. (2014), http://dx.doi.org/10.1016/j.ijplas.2014.03.008.
[167] J. Olbricht, A. Yawny, J.L. Pelegrina, G. Eggeler, et al. J. Alloys Compd. 579 (2013) 249–252.
[168] E. Prokofiev, J. Burow, J. Frenzel, et al. Mater. Sci. Forum 667–669 (2011) 1059–1064.
[169] M. Peterlechner, T. Waitz, C. Gammer, T. Antretter, Int. J. Mater. Res. 6 (2011) 634–642.
[170] J. Burow, E. Prokofiev, C. Somsen, et al. Mater. Sci. Forum 584–586 (2008) 852–857.
[171] Q.S. Mei, L. Zhang, K. Tsuchiya, et al. Scr. Mater. 63 (10) (2010) 977–980.
[172] H.P. Karnthaler, T. Waitz, C. Rentenberger, et al. Mater. Sci. Eng. A 387–389 (2004) 777–782.
[173] T. Waitz, Acta Mater. 53 (8) (2005) 2273–2283.
[174] T. Waitz, W. Pranger, T. Antretter, et al. Mater. Sci. Eng. A 481–482 (2008) 479–483.
[175] T. Waitz, T. Antretter, F.D. Fischer, et al. J. Mech. Phys. Solids 55 (2) (2007) 419–444.
[176] H.S. Liu, L. Mishnaevsky Jr., Comp. Mater. Sci. 76 (2013) 27–36.
[177] A.V. Idesman, V.I. Levitas, D.L. Preston, et al. J. Mech. Phys. Solids 53 (3) (2005) 495–523.
[178] V.I. Levitas, A.V. Idesman, G.B. Olson, Acta Mater. 47 (1) (1998) 219–233.
[179] A.V. Idesman, V.I. Levitas, E. Stein, Comput. Methods Appl. Mech. Eng. 173 (1–2) (1999) 71–98.
[180] A.V. Idesman, V.I. Levitas, D.L. Preston, J.Y. Cho, J. Mech. Phys. Solids 53 (2005) 495–523.
[181] R. Kumazawa, F. Watari, N. Takashi, Y. Tanimura, M. Uo, Y. Totsuka, Biomaterials 23 (2002) 3757–3764.
[182] Y. Mine, S. Makihira, H. Nikawa, H. Murata, R. Hosokawa, A. Hiyama, S. Mimura, J. Prosthodont. Res. 54 (2010) 1–6.
[183] X. Lu, X. Bao, Y. Huang, Y. Qu, H. Lu, Z. Lu, Biomaterials 30 (2009) 141–148.
[184] J.C. Wataha, N.L. O'Dell, B.B. Singh, M. Ghazi, G.M. Whitford, P.E. Lockwood, J. Biomed. Mater. Res. B 58 (2001) 537–544.

[185] M.F. Maitz, N.J. Shevchenko, J. Biomed. Mater. Res. A 76 (2006) 356–365.
[186] L. Tan, R.A. Dodd, W.C. Crone, Biomaterials 24 (2003) 3931–3939.
[187] J.M. Gil, J.A. Manero, J. Planell, F.J. Manero, J.A. Planell, J. Mater. Sci: Mater. Med. 7 (1996) 403–406.
[188] M. Assad, P. Jarzem, M.A. Leroux, C. Coillard, V.A. Chernyshov, C. Charette, C.H. Rivard, J. Biomed. Mater. Res. B. 64B (2003) 107.
[189] L.I. Chu, C.Y. Chung, P.H. Lin, S.D. Wang, Mater. Sci. Eng. A 366 (2004) 114–119.
[190] I. Gotman, Adv. Biomater. 12 (7) (2010) B320–B325.
[191] G. Zorn, A. Lesman, I. Gotman, Oxide Surf. Coat. Technol. 201 (2005) 612–618.
[192] C. Leinenbach, D. Eifler, Biomaterials 27 (2006) 1200–1208.
[193] D. Starosvetsky, I. Gotman, A. Shenhar, J. Mater. Sci.: Mater. Med. 12 (2001) 145–150.
[194] D. Starosvetsky, I. Gotman, Biomaterials 22 (2001) 1853–1859.
[195] G. Meng, Y. Li, F.H. Wang, Electrochim. Acta 51 (2006) 4277–4284.
[196] F.L. Nie, S.G. Wang, Y.B. Wang, S.C. Wei, Y.F. Zheng, Dental Mater. 27 (2011) 677–683.
[197] L. Liu, Y. Li, F. Wang, J. Mater. Sci. Technol. 26 (2010) 1–14.
[198] D. Cheng, V.L. Tellkamp, J. Lavernia, E.J. Lavernia, Ann. Biomed. Eng. 29 (2001) 803–809.
[199] H. Garbacz, M. Pisarek, K.J. Kurzydłowski, Biomol. Eng. 24 (2007) 559–563.
[200] B. Kasemo, J. Prosthetic Dentistry 49 (6) (1983) 832–837.
[201] J. Ryhänen, E. Niemi, W. Serlo, et al. J. Biomed. Mater. Res. 35 (1997) 451–457.
[202] J. Ryhänen, M. Kallioinen, J. Tuukkanen, et al. J. Biomed. Mater. Res. 41 (1998) 481–488.
[203] M. Assad, N. Lemieux, C.H. Rivard, L'.H. Yahia, Bio-Med. Mater. Eng. 9 (1) (1999) 1–12.
[204] R. Bhola, S.M. Bhola, B. Mishra, D.L. Olson, Trends Biomater. Artif. Organs 25 (1) (2011) 34–46.
[205] D.J. Wever, A.G. Veldhuizen, J. de Vries, et al. Biomaterials 19 (7–9) (1998) 761–769.
[206] A.V. Yakubovich, G.B. Sushko, S. Schramm, A.V. Solov'yov, Molecular dynamics simulation of self-diffusion process in titanium in bulk material, on grain junctions and on surface, J. Phys. Chem. A (2014) (under review).
[207] E. Sikora, X.J. Wei, B.A. Shaw, Corrosion 60 (2004) 387–398.
[208] C.Y. Zheng, F.L. Nie, Y.F. Zheng, Y. b, S.C. Cheng, R.Z. Wei, Valiev, Appl. Surf. Sci. 257 (2011) 9086–9093.
[209] E.A. Levashov, M.I. Petrzhik, D.V. Shtansky, Ph.V. Kiryukhantsev-Korneev, A.N. Sheveyko, R.Z. Valiev, D.V. Gunderov, S.D. Prokoshkin, A.V. Korotitskiy, A.Yu. Smolin, Mater. Sci. Eng. A 570 (2013) 51–62.
[210] D.V. Shtansky, E.A. Levashov, I.V. Batenina, N.A. Gloushankova, N.Y. Anisimova, M.V. Kiselevsky, I.V. Reshetov, RSC Adv. 3 (2013) 11107–11115.
[211] D.V. Shtansky, N.A. Glushankova, A.N. Sheveiko, M.A. Kharitonova, T.G. Moizhess, O.V. Malochkin, E.A. Levashov, F. Rossi, Biomaterials 26 (2005) 2909–2924.
[212] D.V. Shtansky, N.A. Gloushankova, I.A. Bashkova, M.I. Petrzhik, A.N. Sheveiko, F.V. Kiryukhantsev-Korneev, E.A. Levashov, I.V. Reshetov, A.S. Grigoryan, Surf. Coat. Technol. 201 (2006) 4111–4118.
[213] D.V. Shtansky, N.A. Glushankova, I.A. Bashkova, M.A. Kharitonova, T.G. Moizhess, A.N. Sheveiko, F.V. Kiruhancev-Korneev, E.A. Levashov, M.I. Petrzhik, Biomaterials 27 (2006) 3519–3531.
[214] C. Auclair-Daigle, M.N. Bureau, J.G. Legoux, L.J. Yahia, J. Biomed. Mater. Res. A 73 (4) (2005) 398–408.
[215] Yu.P. Sharkeev, E.V. Legostaeva, Yu.A. Eroshenko, I.A. Khlusov, O.A. Kashin, Compos. Interface 16 (2009) 535–546.
[216] L. Mishnaevsky Jr., D. Gross, Appl. Mech. Rev. 58 (5) (2005) 338–353.
[217] W.D. Nix, Met. Trans. A 20A (1989) 2217–2245.
[218] J.W. Hutchinson, Z. Suo, in: J.W. Hutchinson, T.Y. Wu (Eds.), Adv. Appl. Mech., vol. 28, 1991, pp. 63–189.
[219] A.G. Evans, J.W. Hutchinson, Acta Metall. Mater. 43 (1995) 2507.
[220] M.D. Thouless, Thin Solid Films 181 (1989) 397–406.
[221] M.D. Thouless, Annu. Rev. Mater. Sci. 25 (1995) 69–96.
[222] R.P. Vinci, J.J. Vlassak, Annu. Rev. Mater. Sci. 26 (1996) 431–462.
[223] S.G. Psakhie, A.Yu. Smolin, Yu.P. Stefanov, P.V. Makarov, M.A. Chertov, Tech. Phys. Lett. 30 (2004) 712–714;
S.G. Psakhie, et al. Phys. Mesomech. 14 (5–6) (2011) 224–248.
[224] J.O. Galante, J. Lemons, M. Spector, P.D. Wilson Jr., T.M. Wright, J. Orthop. Res. 9 (1991) 760–775.
[225] U.W. Bischoff, M.A. Freeman, D. Smith, M.A. Tuke, P.J. Gregson, J. Bone Joint Surg. 76B (1994) 713–716.
[226] K. Hirakawa, T.W. Bauer, B.N. Stulberg, A.H. Wilde, M. Secic, J. Bone Joint Surg. 78A (1996) 1235–1243.
[227] M.J. Pappas, G. Markis, F.F. Buechel, Clin. Orthop. 317 (1995) 64–70.
[228] M.K. Harman, S.A. Banks, W.A. Hodge, J. Arthroplasty 12 (1997) 938–945.
[229] C. Liu, Q. Bi, A. Matthews, Surf. Coat. Technol. 163–164 (2003) 597–604.
[230] I. Gotman, E.Y. Gutmanas, G. Hunter, in: P. Ducheyne, K.E. Healy, D.W. Hutmaher, D.W. Granger, C.J. Kirkpatrick (Eds.), Comprehensive Biomaterials, vol. 1, Elsevier, Oxford, 2011, pp. 127–155 (Chapter 19).
[231] S.N. Massoud, J.B. Hunter, B.J. Holdsworth, W.A. Wallace, R. Juliusson, J. Bone Joint Surg. Br. 79-B (1997) 603–608.
[232] A. Shenhar, I. Gotman, E.Y. Gutmanas, P. Ducheyne, Mater. Sci. Eng. A 268 (1999) 40–46.
[233] A. Shenhar, I. Gotman, S. Radin, P. Ducheyne, E.Y. Gutmanas, Surf. Coat. Technol. 126 (2000) 210–218.
[234] D. Starosvetsky, I. Gotman, Biomaterials 22 (13) (2001) 1853–1859.
[235] G. Sovak, A. Weiss, I. Gotman, J. Bone Joint Surg. Br. 82B (2000) 290–296.
[236] S.J. Wu, E.Y. Gutmanas, I. Gotman, Key Eng. Mater. 434–435 (2010) 481–484.